On Joint Communication and Sensing in Multiple-Input Multiple-Output (MIMO) Wireless Systems

by

Thakshila Perera

A Thesis submitted to The Faculty of Graduate Studies of

The University of Manitoba

in partial fulfillment of the requirements for the degree of

Master of Science

Department of Electrical and Computer Engineering

University of Manitoba

Winnipeg

April 2025

Copyright © Thakshila Perera

Success is not final, failure is not fatal: it is the courage to continue that counts.

Winston Churchill

Abstract

This thesis advances the understanding of integrated beamforming design for joint communication and sensing (JCAS) systems, where a multi-input multi-output (MIMO) base station (BS) supports downlink communication users while simultaneously estimating parameters of a sensing target. The focus is on characterizing the Pareto boundary between communication performance (measured by mutual information (MI), sum-rate capacity) and sensing performance (measured by Fisher information (FI)), subject to practical system constraints. Two key scenarios are investigated: (1) a single-user, single-sensing-object system with and without equivalent isotropic radiated power (EIRP) constraints, and (2) a multi-user, single-sensing-object system, both subject to a total transmit power budget.

In the single-user scenario without EIRP constraints, a closed-form solution is derived for the Pareto-optimal beamforming design, which is parameterized by a single scalar variable governing the trade-off between MI/sum-rate and FI. This solution is validated against iterative algorithms (e.g., projected gradient descent) and convex optimization (CVX) frameworks, demonstrating its optimality. For the EIRP-constrained case, the problem is reformulated using Lagrangian and Karush-Kuhn-Tucker conditions, and solved via a customized gradient descent algorithm. The results confirm that joint beamforming outperforms independent strategies, with the Pareto boundary influenced by the user's and target's angles of departure (AoD), antenna configurations, and EIRP limits.

In the multi-user scenario, uplink-downlink duality is used to decouple the multi-objective optimization problem. Through Lagrangian methods and block-coordinate ascent, an efficient algorithm is developed to maximize the weighted sum of MI/sum-rate across users and FI for sensing. This approach shows that joint beamforming

remains Pareto-optimal, efficiently allocating resources to mitigate interference while enhancing sensing accuracy.

Numerical evaluations across various configurations validate the theoretical findings, revealing that EIRP constraints tighten the Pareto boundary, highlighting the need for adaptive power allocation strategies in practical systems.

This work provides a foundation for designing next-generation JCAS systems, emphasizing integrated beamforming as a means to harmonize communication and sensing objectives. The derived frameworks and numerical tools offer valuable insights for optimizing MIMO-based dual-functional networks in applications such as vehicular radar-communication coexistence and 6G perceptive networks.

Keywords: Joint Communication and Sensing (JCAS), Pareto Boundary, Mutual Information (MI), Sum-rate, Fisher Information (FI), Equivalent Isotropic Radiated Power (EIRP), joint beamforming, uplink-downlink duality.

Acknowledgment

This thesis represents the culmination of two years of dedicated effort and perseverance. I could not have completed this journey without the unwavering support of some incredible individuals. It is a privilege to extend my heartfelt gratitude to all of them at this moment.

First, I express my profound gratitude to my supervisor, Professor Ekram Hossain, for allowing me to join his research group and for his support, guidance, and encouragement throughout this journey. His confidence in my abilities and exceptional mentorship have been pivotal in advancing this research and fostering my academic development.

I am deeply grateful to Professor Amine Mezghani for his invaluable feedback, thoughtful insights, and the generous time he devoted to reviewing my work. His guidance and constructive feedback have been essential to improve the quality of this research. I would also like to express my deep appreciation to the committee member, Professor Sherif Sherif, for his expert guidance and feedback, which have been essential in strengthening this study.

I am deeply grateful to my family, whose unconditional love and sacrifices have been the cornerstone of my accomplishments. To my husband: Your patience, understanding, and unwavering support have been a constant source of strength and inspiration throughout this journey.

Finally, I would like to thank all my friends, both from university and beyond, for their constant support, encouragement, and companionship throughout this journey. Special thanks to Inuri and Gaveen for always being there for me.

Table of Contents

Table of Contents **v**

List of Figures **viii**

List of Tables **x**

List of Abbreviations **xii**

1 Introduction **1**

1.1 Overview 1

1.1.1 Joint Communication and Radar (C&R) Systems 2

1.1.2 Fisher Information (FI) 4

1.1.3 Mutual Information (MI) 5

1.1.4 Equivalent Isotropic Radiated Power (EIRP) 6

1.2 Motivation 7

1.3 Contribution 9

1.3.1 Characterizing the Pareto Boundary for JCAS in a Single-User MIMO System 9

1.3.2 Characterizing the Pareto Boundary for JCAS in a Multi-User MIMO System 11

1.4 Summary of Academic Contributions and Key Achievements 12

1.5 Thesis Outline and Notations 12

2 Characterizing the Pareto Boundary for JCAS in a Single-User MIMO System 15

2.1 System Model and Assumptions 15

2.1.1 Signal Model 16

2.1.2 MI for the Single Communication User 17

2.1.3 FI for Sensing Object 17

2.2 Problem Formulation and Solution Approach - Without EIRP Limitations 18

2.2.1 Problem Formulation 19

2.2.2 Proposed Solution - Closed-form Solution 19

2.2.3 Proposed Solution - PGD Solution 22

2.3 Problem Formulation and Solution Approach - With EIRP Limitations . 27

2.3.1 Problem formulation 27

2.3.2 Proposed Solution 27

2.3.3 Analysis of Computational Complexity 30

2.4 Simulation Results 31

2.4.1 Simulation Parameters 31

2.4.2 Without EIRP Limitations 32

2.4.3 With EIRP Limitations 37

2.5 Chapter Summary 41

3 Characterizing the Pareto Boundary for JCAS in a Multi-User MIMO System 43

3.1 System Model and Assumptions 43

3.1.1 Signal Model 44

3.1.2 MI for the Communication User 46

3.1.3 FI for Sensing Object 47
3.2 Problem Formulation 48
3.3 Solution Approach 50
3.3.1 Analysis of Computational Complexity 52
3.4 Simulation Results 54
3.4.1 Simulation Parameters 55
3.5 Chapter Summary 63

4 Conclusion and Future Directions **65**
4.1 Conclusion 65
4.2 Future Works 67
4.2.1 Advanced Optimization Methods 67
4.2.2 Multi-User Multi-Target JCAS Scenarios 67
4.2.3 Near-Field JCAS Systems 68
4.2.4 JCAS in Integrated Satellite-Terrestrial Networks (ISTN) 68
4.2.5 JCAS for Vehicular and Autonomous Systems 69

Appendices: **70**

A Derivation of the FIM **70**

B Proof of Proposition 3.1 **72**

C BC to MAC Transformation **74**

Bibliography **76**

List of Figures

2.1 Single-user MIMO JCAS System Model. 16

2.2 Variation of the tr($\mathbf{R}_{\mathbf{x}}$) with the Lagrange multiplier. 21

2.3 Comparison between joint and separate beamforming for communication and sensing in terms of the trade-off between mutual information and Fisher information. 32

2.4 Closed-form rank-one solution and numerical (using CVX toolbox) solution for different values of N_r and N_t. 34

2.5 PGD solution and numerical (using CVX toolbox) solution. 35

2.6 Variation of the trade-off with AoD of the user with $N_r = 4$ and $N_t = 4$. 35

2.7 Variation of the trade-off with (a) the number of transmitting antennas, (b) the number of receiving antennas. 36

2.8 Comparison between numerical and PGD solutions for different N_r and N_t values. 38

2.9 Comparison between the communication and sensing performance trade-off with EIRP values user at $\pi/6$. 39

2.10 Comparison between the communication and sensing performance trade-off with EIRP values user at $\pi/2$. 40

3.1 Joint communication and sensing model of MIMO BC. 44

3.2 Comparison between optimal and sub-optimal beamforming for various numbers of users in terms of the trade-off between sum rate and Fisher Information 57
3.3 Comparison between optimal and sub-optimal beamforming for various numbers of transmitting and receiving antennas in terms of the trade-off between sum-rate and Fisher Information 58
3.4 Variation of trade-off with number of communication users 59
3.5 Variation of trade-off with transmit power budget 60
3.6 Variation of trade-off with number of transmitting antennas 61
3.7 Variation of trade-off with number of receiving antennas 62

List of Tables

1.1 Summary of Academic Publications and Contributions 13

3.1 Simulation parameters and values 56

List of Abbreviations

IoT	Internet of Things
CRSS	Communication and Radar Spectrum Sharing
CRC	Coexistence Radar and Communication
C&R	Communication and Radar
JRC	Joint Radar Communication
DFRC	Dual-Function Radar Communication
RadCom	Integrated Radar and Communication
JCAS	Joint Communication and Radar/Radio Sensing
FI	Fisher Information
MLE	Maximum Likelihood Estimation
CRB	Cram´er-Rao Bound
PDF	Probability Density Function
CRLB	Cram´er-Rao Lower BounD
FIM	Fisher Information Matrix
MI	Mutual Information
SINR	Signal to Interference plus Noise Ratio
EIRP	Equivalent Isotropic Radiated Power
MIMO	Multiple Input Multiple Output
ISAC	Integrated Sensing and Communication

FDSAC	Frequency-Division Sensing and Communication
BS	Base Station
PGD	Projected Gradient Descent
KKT	Karush-Kuhn-Tucker
AoD	Angle of Departure
AoA	Angle of Arrival
BC	Broadcast Channel
MAC	Multiple-Access Channel
UAV	Unmanned Aerial Vehicle
LOS	Line-of-Sight
NLOS	Non-Line-of-Sight
AWGN	Additive White Gaussian Noise
ULA	Uniform Linear Array
SVD	Singular Value Decomposition
EVD	Eigen Value Decomposition
RIS	Reconfigurable Intelligent Surfaces
ISTN	Integrated Satellite-Terrestrial Networks
CSI	Channel State Information
HAPS	High-Altitude Platform Systems
V2X	Vehicle-to-Everything

Chapter 1

Introduction

1.1 Overview

Next-generation wireless networks, including 6G and beyond, aim to revolutionize communication by addressing the growing demand for high-performance services and the increasing proliferation of Internet of Things (IoT) devices. These future networks are expected to support applications such as intelligent transportation and smart homes, which require not only superior wireless connectivity but also robust sensing capabilities [1–3]. However, efficiently utilizing wireless spectrum and hardware resources remains a significant challenge. Researchers have explored communication and radar spectrum sharing (CRSS) to address this, where radar and communication systems operate within a shared spectral environment. By utilizing the compatible portion of radar frequencies, CRSS provides an efficient way to integrate wireless communication and sensing [4]. In general, CRSS can be categorized into three main types: coexistence radar and communication (CRC), cooperative radar and communication, and joint communication and radar (C&R) [5,6]. The CRC approach requires radar and communication transceivers to treat each other as interference sources, meaning no information

is shared between the systems. As a result, each system must independently estimate and mitigate interference [7–9]. In contrast, the cooperative radar and communication method allows for partial information sharing, enabling more effective interference mitigation. Here, the two systems no longer function as interferences but instead use shared knowledge to enhance overall performance [5, 10]. Joint C&R is particularly appealing among these approaches as it fully integrates radar and communication functionalities within a single system.

1.1.1 Joint Communication and Radar (C&R) Systems

Incorporating joint C&R into wireless networks improves spectrum efficiency, coverage, and signal quality by dynamically managing resources and optimizing beamforming using real-time environmental data [11–14]. It also enhances energy efficiency by intelligently scheduling communication and sensing tasks while strengthening network security and privacy through real-time threat detection and anomaly monitoring. Moreover, JCAS supports advanced applications such as autonomous navigation, augmented reality, and smart city solutions, accelerating consumer adoption and unlocking the full potential of 5G technology [15].

Integration of communication and radar into a single system can be classified into two categories: (1) the two functions coexist within a single system but operate using distinct hardware components and/or separate waveforms, which can be combined or allocated across different time, frequency, or spatial domains [9,16]; (2) the integration of both functions via shared hardware components, utilizing a singular waveform optimized to augment both communication and sensing capabilities [17, 18]. The first category signifies a loose integration, offering only limited advantages such as reduced signaling overhead and interference mitigation, while the second category marks a substantial progression beyond collocation. Moreover, based on the design priorities, joint C&R

systems can be classified into three categories [19, 20]:

1. *Communication centric design*: Radar sensing serves as an extension to a communication system, where the main priority is communication [21–23]. The goal is to utilize the communication waveform to extract radar information from target reflections. This requires advancements in both hardware and algorithms to enable radar sensing. Adjustments to communication standards could be made to better facilitate the reuse of the communication waveform for radar sensing. In this setup, communication performance is generally unaffected, though the radar sensing performance may depend on the specific scenario and could be difficult to optimize [24].

2. *Radar-centric design*: These approaches focus on modulating or embedding information signals into an existing radar waveform [25–27]. Since the radar signaling remains mostly unchanged, these approaches can achieve near-optimal radar performance. However, the main disadvantage is that they result in limited data rates. To improve communication capabilities, some performance trade-offs in radar functionality may be acceptable [9]. One benefit is that long-range communication is possible due to the high transmission power of radar systems [20].

3. *Joint design and optimization*: This category includes systems that are designed jointly from the outset to allow a flexible trade-off between C&R performance. These systems may not be restricted by existing communication or radar standards [20].

Research on joint C&R systems has been explored under various terminologies, such as joint radar communication (JRC) [28, 29], dual-function radar communication (DFRC) [30, 31], integrated radar and communication (RadCom) [32–34], and joint communication and radar/radio sensing (JCAS) [18, 35, 36]. This study adopts the term JCAS

to reflect the joint optimization of communication and sensing functionalities in an integrated system, aligning with the holistic perspective central to this research.

1.1.2 Fisher Information (FI)

FI is a fundamental concept in statistics and information theory that quantifies the amount of information an observable random variable X carries about an unknown parameter θ upon which its probability distribution depends. It plays a critical role in parameter estimation, particularly in maximum likelihood estimation (MLE) and in establishing the Cramér-Rao bound (CRB) [37].

Mathematical Definition

Consider a probability density function (PDF) $f(X;\theta)$. The natural logarithm of the PDF is denoted as $\ln f(X;\theta)$. The Fisher Information $\mathrm{I}(\theta)$ is then defined as:

$$\mathrm{I}(\theta) = \mathbb{E}\left[\left(\frac{\partial}{\partial\theta}\ln f(X;\theta)\right)^2\right] = -\mathbb{E}\left[\frac{\partial^2}{\partial\theta^2}\ln f(X;\theta)\right]. \tag{1.1}$$

When the parameter θ is a vector, i.e., $\theta = (\theta_1, \theta_2, \ldots, \theta_N)^T$, the Fisher Information generalizes to a matrix known as the FI Matrix (FIM). The FIM is an $N \times N$ matrix, where each element is given by:

$$[\mathbf{I}(\theta)]_{ij} = \mathbb{E}\left[\left(\frac{\partial}{\partial\theta_i}\ln f(X;\theta)\right)\left(\frac{\partial}{\partial\theta_j}\ln f(X;\theta)\right)\right] = -\mathbb{E}\left[\frac{\partial^2}{\partial\theta_i\partial\theta_j}\ln f(X;\theta)\right]. \tag{1.2}$$

Cramér-Rao Lower Bound (CRLB)

The CRLB is a theoretical lower bound on the variance of any unbiased estimator $\hat{\theta}$ of the parameter θ. It provides a fundamental limit on the precision of unbiased estimation and is derived using the Fisher Information [38]. The CRLB is expressed as:

$$\mathrm{Var}(\hat{\theta}) \geq \frac{1}{\mathbf{I}(\theta)}. \tag{1.3}$$

This inequality indicates that the variance of any unbiased estimator cannot be smaller than the inverse of the FI. Thus, higher FI corresponds to greater precision in parameter estimation.

FI in JCAS Systems

FI and/or CRLB are critical tools in JCAS systems. They enable the evaluation and optimization of sensing performance while maintaining efficient communication capabilities. Specifically, FI facilitates the design of beamforming strategies that balance sensing accuracy (e.g., target localization, angle-of-arrival estimation) and communication efficiency (e.g., throughput, spectral efficiency), ensuring seamless coexistence of both functionalities without mutual performance degradation. Furthermore, FI serves as the cornerstone for system optimization and performance analysis in multi-antenna JCAS architectures [39, 40].

1.1.3 Mutual Information (MI)

MI, a foundational concept in information theory, quantifies the statistical dependence between two or more random variables [41]. Initially introduced by Shannon, MI continues to serve as a critical tool in analyzing relationships in data across a variety of applications. For two given random variables s and y, the MI is $I(s;y)$ quantifies the reduction in uncertainty (entropy) of one variable given knowledge of the other and vice versa. It captures both linear and nonlinear dependencies. MI is non-negative, with equality holding if and only if the random variables are independent. Moreover, it is symmetric, meaning $I(s;y) = I(y;s)$ [42]. In wireless communication, channel capacity refers to the maximum rate at which information can be transmitted over a communication channel with an arbitrarily small probability of error. This represents the upper bound on the amount of information that can be reliably transmitted. According to

Shannon's theorem, the capacity $\mathcal{C}$ of a communication channel is the maximum mutual information between the input and the output, where the input signal is optimized to maximize the mutual information for a given channel [43]. The channel capacity is given by:

$$\mathcal{C} = \max_{\text{signal constraints}} I(s; y). \tag{1.4}$$

Shannon's capacity formula can also be expressed in terms of the signal-to-interference plus noise ratio (SINR):

$$\mathcal{C} = \log_2(1 + \text{SINR}). \tag{1.5}$$

This formula demonstrates that as the SINR increases, the MI (and consequently the capacity) also increases, as a higher SINR means a stronger signal relative to noise and interference, leading to more information being successfully transmitted.

MI in JCAS systems

In JCAS systems, MI plays a crucial role in optimizing the trade-off between communication and sensing functions [17]. MI quantifies the amount of information that can be transmitted or sensed over a shared channel, serving as a performance metric for both aspects. It helps maximize communication capacity by guiding resource allocation (e.g., power, beamforming) while improving sensing accuracy, particularly in tasks like target detection and tracking [44]. MI is vital to designing optimal beamforming strategies and managing interference, ensuring efficient use of resources. By analyzing MI, JCAS systems can effectively balance communication and sensing objectives, leading to better overall performance.

1.1.4 Equivalent Isotropic Radiated Power (EIRP)

EIRP is a crucial parameter for describing transmitting antennas. It measures the power radiated by an antenna, considering both the transmitter's output power and the

antenna gain in a specific direction [45]. EIRP represents the total radiated power as if it were emitted isotropically (equally in all directions) while maintaining the same maximum power density. Mathematically, it is expressed as:

$$\text{EIRP} = P_t \cdot G_a \tag{1.6}$$

where P_t is the transmitted power (in watts or dBm), and G_a is the antenna gain (dimensionless or in dBi, referring to gain relative to an isotropic radiator).

EIRP plays a vital role in wireless communication, influencing the received signal strength, coverage, interference, and system performance. In multiple input multiple output (MIMO) JCAS systems, EIRP is particularly important in single-beam transmission, where it helps:

- Ensure regulatory compliance by limiting excessive radiated power.
- Optimize coverage and signal quality by maximizing power in desired directions.
- Manage interference with neighboring systems.
- Enhance sensing performance by improving signal detectability.

However, in multi-user scenarios, EIRP is less critical because the system transmits multiple beams, distributing the total power among different users. Instead of maximizing the power in a single direction, the system focuses on beamforming gain, power allocation, and interference management to optimize overall performance. Thus, while EIRP remains an essential metric, its significance varies depending on the transmission scheme and system objectives.

1.2 Motivation

Recent studies on MIMO JCAS systems have primarily focused on optimizing either communication or sensing performance using MI or CRB. Several works have explored

CRB minimization while ensuring SINR constraints for communication [29, 46]. However, more recent efforts have shifted toward analyzing the CRB-rate trade-off, establishing the Pareto boundary between communication and sensing [47, 48]. While these works provide valuable insights, they do not fully capture the interaction between MI and FI in MIMO JCAS systems.

On the other hand, MI is widely used as a communication performance metric, particularly in multi-user and multi-channel scenarios, where sum-rate capacity represents the maximum achievable data rate across all users [42]. MI has been employed to analyze the trade-off between communication and sensing in various integrated sensing and communication (ISAC) models, including Gaussian ISAC channels [49], frequency-division sensing and communication (FDSAC) [50], and uplink-downlink scenarios [51,52]. However, these studies primarily focus on MI-based optimization and do not consider FI as the sensing metric when establishing the communication-sensing trade-off.

Additionally, the uplink-downlink duality principle has been effectively used to simplify beamforming design in MIMO communication systems [53–55]. Recent work has leveraged this concept in ISAC [56], optimizing sensing performance while maintaining communication quality. However, the relationship between MI and FI in uplink-downlink duality for JCAS remains largely unexplored.

Given these considerations, we are motivated to characterize the Pareto boundary for JCAS using MI as the communication performance metric and FI as the sensing performance metric. Furthermore, the uplink-downlink duality between MI and FI in MIMO JCAS systems serves as an additional key motivation for our research. Within this framework, the Pareto boundary provides a crucial benchmark for practical implementations, as it captures the trade-offs between MI and FI.

1.3 Contribution

This section is divided into two parts, each addressing a single sensing object:

- Optimization of joint beamforming in a JCAS-enabled MIMO base station (BS) with a single communication user, both with and without considering the effect of EIRP.
- Optimization of joint beamforming in a JCAS-enabled MIMO BS with multiple communication users.

Additionally, for both cases, we characterize the Pareto boundary between communication and sensing performance.

1.3.1 Characterizing the Pareto Boundary for JCAS in a Single-User MIMO System

We propose a method to optimize joint beamforming for communication and sensing in a MIMO wireless system, considering a single downlink communication user. We also account for the effect of EIRP on the communication user. Specifically, we analyze two cases: (1) Without EIRP limitations, and (2) With EIRP limitations. Our key contributions are as follows:

- **Multi-Objective Optimization**: We formulate a multi-objective optimization problem to simultaneously maximize two critical performance metrics: MI and FI. This optimization is subject to a transmit power budget, ensuring the total power does not exceed a predefined limit. We investigate two distinct scenarios: one without EIRP constraints and one with EIRP limitations. This dual-scenario approach provides insight into the trade-offs between communication and sensing performance.

- **Optimization without EIRP Limitations**: For Case 1 (without EIRP limitations), we derive a closed-form optimal solution using Lagrangian optimization techniques. This yields a solution expressed in terms of a single scalar parameter. We refine this parameter using a line search method to iteratively converge to the optimal point under the given constraints.

- **Optimization with EIRP Limitations**: For Case 2 (with EIRP limitations), the optimization problem becomes more complex due to the additional constraints. To solve this, we employ an iterative algorithm based on projected gradient descent (PGD). We integrate the Karush-Kuhn-Tucker (KKT) conditions to verify that the necessary optimality conditions are met at convergence. This combined approach enables us to handle the complex constraints and converge to an optimal solution that satisfies both the power budget and EIRP limitations.

- **Pareto Boundary Analysis**: For both cases, we derive and analyze the Pareto boundary, which captures the inherent trade-offs between communication and sensing performance. The Pareto boundary represents the set of optimal operating points, where any improvement in MI comes at the expense of a reduction in FI, and vice versa. This analysis provides valuable insights into how system parameters can be adjusted to balance communication capacity and sensing accuracy in JCAS MIMO systems.

- **Case 1 Insights**:

  - We compare joint beamforming with separate beamforming strategies for JCAS systems, highlighting the differences in their respective Pareto boundaries.

  - We explore the impact of varying the user's AoD on the Pareto boundary while keeping the number of transmit and receive antennas fixed.

  - We analyze how the number of transmit and receive antennas affects the Pareto boundary, shedding light on how system dimensions influence the communication-sensing trade-off.

- **Case 2 Insights**: In this case, we focus on the effect of EIRP limitations, examining how these constraints modify the trade-off between communication and sensing performance.

1.3.2 Characterizing the Pareto Boundary for JCAS in a Multi-User MIMO System

Building on the previous work, we propose a method for optimizing joint beamforming for communication and sensing in a MIMO system with multiple downlink communication users. Our contributions are as follows:

- **Optimization Framework**: We formulate an optimization problem similar to the previous case, but instead of modeling the system as a MIMO broadcast channel (BC), we adopt a MIMO multiple-access channel (MAC) framework. This formulation allows us to derive the MIMO sum-rate capacity, defined as the sum of the MI across all users. We explore two beamforming strategies for communication and sensing, which are critical to understanding the system's performance.

- **Beamforming Strategy**: We mathematically demonstrate that a dedicated sensing beam is not necessary to achieve the maximum weighted sum of FI and sum-rate capacity. Instead, a joint beamforming strategy is more effective, optimally utilizing available resources to enhance both communication and sensing performance. This insight simplifies the optimization problem.

- **Optimization Techniques**: Similar to Case 1, we derive a numerical closed-form solution for each user, expressed as a scalar, using Lagrangian optimization and

line search methods. We use block coordinate ascent to iteratively optimize one variable at a time, while keeping others fixed, to efficiently solve the optimization problem. To determine the optimal downlink covariance matrices, we convert the MAC to BC for each user, ensuring effective resource allocation.

- **Simulation Results**: Our main simulation results compare optimal and sub-optimal beamforming strategies, examining the trade-off between sum-rate capacity and FI. We investigate the impact of various system parameters—such as the number of communication users, transmit and receive antennas, and transmit power budget on the communication-sensing trade-off. Specifically, we analyze how these parameters affect the system's ability to achieve an optimal balance between communication and sensing. These findings provide valuable insights for the design and optimization of multi-user MIMO JCAS systems.

1.4 Summary of Academic Contributions and Key Achievements

This thesis includes content that has been previously published conference and submitted to a peer-reviewed journal, contributing to the academic discourse in the field. A summary of these publications and submissions is provided in Table 1.1.

1.5 Thesis Outline and Notations

We organize the rest of this thesis as follows:

- In Chapter 2, we conduct an analysis of joint beamforming optimization in a MIMO JCAS system with a single communication user and a single sensing object, considering both cases with and without EIRP limitations. Section 2.1 presents

Table 1.1: Summary of Academic Publications and Contributions

Publications	**Appearance**
1. **T. Perera**, A. Mezghani, E.Hossain, "On the Characterization of Pareto Boundary for Joint Communication and Sensing in MIMO Wireless Systems," in *2024 IEEE International Conference on Communications Workshops (ICC Workshops)*, pp. 685-690, doi: 10.1109/ICCWorkshops59551.2024.10615441.	Chapter 2
2. **T. Perera**, A. Mezghani, E.Hossain, "A Multi-Objective Approach to Joint Communication and Sensing: Characterizing the Pareto Boundary in Multi-user MIMO Systems" submitted to *IEEE Transactions on Wireless Communications*.	Chapter 2 , Chapter 3

the system model and outlines the key assumptions. The optimization problem and solution methodology for the case "without EIRP limitations" are detailed in Section 2.2. Section 2.3 provides the optimization problem and solution methodology for the case "with EIRP limitations." Finally, Section 2.4 discusses the simulation results for both scenarios.

- In Chapter 3, we examine joint beamforming optimization in a MIMO JCAS system with multiple communication users and a single sensing object. Section 3.1 presents the system model and outlines the assumptions. The problem formulation is provided in Section 3.2, while the solution approach is discussed in Section 3.3. Finally, Section 3.4 presents the simulation results.

- In Chapter 4 includes the conclusions and discusses potential directions for future research. Furthermore, detailed derivations are provided in the Appendix.

Notations: Vectors and matrices are denoted by small boldface letters (e.g., $\mathbf{v}$) and capital boldface letters (e.g., $\mathbf{X}$), respectively. $\mathbb{C}^{N\times M}$ denotes the space of $N \times M$ complex matrices. $\mathbf{I}$ represents the identity matrix with appropriate dimensions. For a square matrix $\mathbf{A}$, $\mathrm{tr}(\mathbf{A})$ denotes its trace , $\mathbf{A} \succeq 0$ means that $\mathbf{A}$ is positive semi-definite and $\mathbf{A} \preceq 0$ denotes that $\mathbf{A}$ is negative semi-definite while $\mathtt{rank}(\mathbf{A})$ denotes the rank of the matrix. For any arbitrary complex matrix $\mathbf{B}$, $\mathbf{B}(i,j)$, $\mathrm{rank}(\mathbf{B})$, $\mathbf{B}^T$, $\mathbf{B}^H$, and $\mathbf{B}^*$ denotes its $(i,j)^{th}$ element, rank, transpose, conjugate transpose, and complex conjugate respectively. $\mathbb{E}(\cdot)$ denotes the statistical expectation. $||\cdot||$ is the Euclidean norm of a vector, $||\cdot||_{\mathbf{F}}$ is the Frobenius norm of a matrix, and $|\cdot|$ is the absolute value.

Chapter 2

Characterizing the Pareto Boundary for JCAS in a Single-User MIMO System

2.1 System Model and Assumptions

We consider a MIMO terrestrial BS with an array of N_t transmitting antennas and an array of N_r receiving antennas, enabling JCAS performance. This setup also includes a downlink communication user with a single antenna and a sensing object, such as an unmanned aerial vehicle (UAV), as depicted in Fig.2.1. To enhance the sensing performance independently of the downlink performance, we use multiple (N_r) receiving antennas. The downlink channel to the user includes multipath components, including a Line-of-Sight (LOS) path and Non-Line-of-Sight (NLOS) signals. We assume that only a LOS signal is present for the sensing object. Moreover, we consider all types of interferences and noises as additive white Gaussian noise (AWGN).

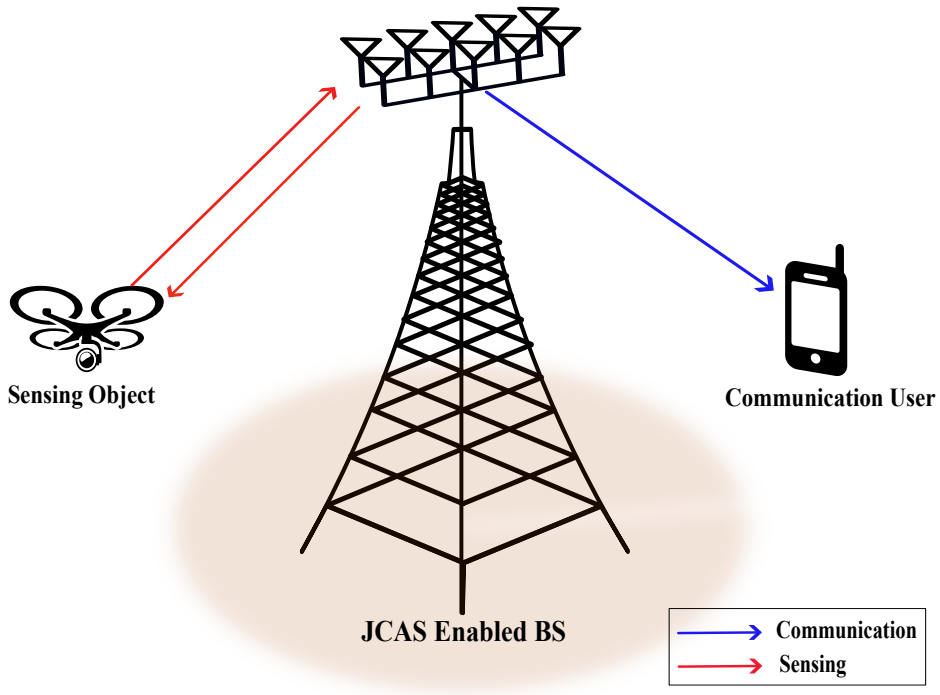


Figure 2.1: Single-user MIMO JCAS System Model.

2.1.1 Signal Model

The JCAS signal from the BS is represented as $\mathbf{x} \in \mathbb{C}^{N_t}$. We define the JCAS transmit covariance matrix $\mathbf{R_x} \in \mathbb{C}^{N_t \times N_t}$ as

$$\mathbf{R_x} = \mathbb{E}[\mathbf{x}\mathbf{x}^H], \tag{2.1}$$

with the total power constraint $\text{tr}(\mathbf{R_x}) \leq P_{tx}$. The received signal by the communication user is

$$y_c = \mathbf{h}^H \mathbf{x} + z_c, \tag{2.2}$$

where $\mathbf{h}^H \in \mathbb{C}^{1 \times N_t}$ is the communication channel vector. The random variable $z_c \in \mathbb{C}$ is the AWGN with zero mean and σ_c^2 variance. On the sensing side, the reflected echo signal at the BS when transmitting the $\mathbf{x}$ to sense the sensing object is

$$\mathbf{y}_r = \mathbf{G}\mathbf{x} + \mathbf{z}_r, \tag{2.3}$$

where $\mathbf{z}_r \in \mathbb{C}^{N_r}$ is the AWGN with zero mean and σ_r^2 variance for each. $\mathbf{G} \in \mathbb{C}^{N_r \times N_t}$ denotes the target response matrix and for a single target case it can be represented as

$$\mathbf{G} = \gamma_r \mathbf{b}(\theta_r)\mathbf{a}^T(\theta_r), \tag{2.4}$$

where $\gamma_r \in \mathbb{C}$ is the reflection coefficient which includes both radar cross-section and round trip path-loss and θ_r is the angle of the sensing object relative to the BS. The vectors $\mathbf{a}(\theta_r) \in \mathbb{C}^{N_t}$ and $\mathbf{b}(\theta_r) \in \mathbb{C}^{N_r}$ denote the transmit and receive array response vectors, respectively. In our case, the angle of arrival (AoA) and angle of departure (AoD) are equal (monostatic radar).

2.1.2 MI for the Single Communication User

For Gaussian transmit vector $\mathbf{x}$, MI can be expressed as

$$\text{MI} = \log_2\left(1 + \frac{\mathbf{h}^H \mathbf{R}_\mathbf{x} \mathbf{h}}{\sigma_c^2}\right). \tag{2.5}$$

2.1.3 FI for Sensing Object

Consider the observation model in (2.3). Since vector $\mathbf{x}$ is known at the base station, the FI matrix, $\mathbf{J}$ for the estimating vector, $\mathbf{v} = [\theta_r \quad \gamma_r \quad \gamma_r^*]^T$ can be formulated as follows (note that we have a mixture of real and complex parameters and all parameters are dimensionless)(see **AppendixA**):

$$\mathbf{J} = \frac{1}{\sigma_r^2}\begin{bmatrix} J_{(1,1)} & J_{(1,2)} & J_{(1,3)} \\ J_{(2,1)} & J_{(2,2)} & 0 \\ J_{(3,1)} & 0 & J_{(3,3)} \end{bmatrix}, \tag{2.6}$$

with

$$J_{(1,1)} = 2\gamma_r^* \gamma_r \,\text{tr}(\dot{\mathbf{A}}\mathbf{R}_\mathbf{x}\dot{\mathbf{A}}^H) \tag{2.7}$$

$$J_{(2,2)} = \text{tr}(\mathbf{A}\mathbf{R}_\mathbf{x}\mathbf{A}^H) \tag{2.8}$$

$$J_{(3,3)} = \text{tr}(\mathbf{A}\mathbf{R}_{\mathbf{x}}\mathbf{A}^H) \tag{2.9}$$

$$J_{(1,2)} = J_{(2,1)} = \gamma_r^* \,\text{tr}(\mathbf{A}\mathbf{R}_{\mathbf{x}}\dot{\mathbf{A}}^H) \tag{2.10}$$

$$J_{(1,3)} = J_{(3,1)} = \gamma_r \,\text{tr}(\dot{\mathbf{A}}\mathbf{R}_{\mathbf{x}}\mathbf{A}^H). \tag{2.11}$$

where $\dot{\mathbf{A}} = \frac{\partial \mathbf{A}}{\partial \theta_r}$ and $\mathbf{A} = \mathbf{b}(\theta_r)\mathbf{a}^T(\theta_r)$.

Considering the origin to be located at the center of the uniform linear array (ULA) [57, 58], then, the transmit array response vector and its derivative w.r.t. θ_r can be written as follows:

$$\mathbf{a}\left(\theta_r\right) = \left[e^{-j\frac{N_t-1}{2}k\sin\theta_r}, e^{-j\frac{N_t-3}{2}k\sin\theta_r}, \ldots, e^{j\frac{N_t-1}{2}k\sin\theta_r}\right]^T \tag{2.12}$$

$$\dot{\mathbf{a}}\left(\theta_r\right) = \left[-ja_1\frac{N_t-1}{2}k\cos\theta_r, \ldots, -ja_{N_t}\frac{N_t-1}{2}k\cos\theta_r\right]^T, \tag{2.13}$$

where $k = \frac{2\pi d}{\lambda}$, d is the distance between two adjacent antennas in the array, λ is the wavelength, and $\mathbf{a}_i$ represents the i^{th} element in of $\mathbf{a}\left(\theta_r\right)$. Similarly we can express $\mathbf{b}\left(\theta_r\right)$ and $\dot{\mathbf{b}}\left(\theta_r\right)$ for the receiving array.

2.2 Problem Formulation and Solution Approach - Without EIRP Limitations

In this section, we discuss the optimization problem for a single-user single-sensing object scenario as described in Section 2.1 without considering the effect of EIRP limitations. We develop a closed-form solution for this case. In terms of sensing performance metric, we use the trace of the FI matrix due to mathematical tractability and motivated by the fact that the parameters γ_r and θ_r are not strongly coupled and the FI matrix is mainly diagonal.

2.2.1 Problem Formulation

Our objective is to maximize the weighted sum of FI and MI to design the beamforming at the BS under the power budget constraint. The problem is formulated as follows:

$$\text{P1}: \underset{\mathbf{R_x}}{\text{maximize}} \quad \alpha \,\text{tr}(\mathbf{J}) + (1-\alpha)\text{MI} \tag{2.14a}$$

$$\text{subject to}$$

$$C1: \text{tr}(\mathbf{R_x}) \leq P_{tx}, \tag{2.14b}$$

$$C2: \mathbf{R_x} \succeq 0, \tag{2.14c}$$

where $\text{tr}(\mathbf{J}) = \frac{2}{\sigma_r^2}(\gamma_r^* \gamma_r \,\text{tr}(\dot{\mathbf{A}}\mathbf{R_x}\dot{\mathbf{A}}^H) + \text{tr}(\mathbf{A}\mathbf{R_x}\mathbf{A}^H))$, α is the weighting coefficient and the MI is given by (2.5). P_{tx} is transmit power budget. Then, the optimization problem can be restated as follows:

$$\underset{\mathbf{R_x}}{\text{maximize}} \quad \frac{2\alpha}{\sigma_r^2}\gamma_r^*\gamma_r \,\text{tr}(\dot{\mathbf{A}}\mathbf{R_x}\dot{\mathbf{A}}^H) + \frac{2\alpha}{\sigma_r^2}\,\text{tr}(\mathbf{A}\mathbf{R_x}\mathbf{A}^H) + (1-\alpha)\log_2\left(1 + \frac{\mathbf{h}^H\mathbf{R_x}\mathbf{h}}{\sigma_c^2}\right) \tag{2.15a}$$

subject to

$$\text{C1}: \text{tr}(\mathbf{R_x}) \leq P_{tx}, \tag{2.15b}$$

$$\text{C2}: \mathbf{R_x} \succeq 0. \tag{2.15c}$$

2.2.2 Proposed Solution - Closed-form Solution

The problem in (2.15) is a convex optimization problem. As a result, we can directly employ numerical convex tools such as CVX [59] to solve it. However, here, our objective is to find a closed-form solution to the problem. To obtain the closed-form solution for $\mathbf{R_x}$, we use the Lagrange optimization technique with a fixed constraint on the power

budget. The corresponding Lagrangian optimization of (2.15) can be reformulated as follows (while ignoring the matrix inequality constraint C2 at this point):

$$\text{P2}: \underset{\mathbf{R}_{\mathbf{x}}^{'}}{\text{maximize}} \ \frac{(1-\alpha)}{\ln 2}\ln(1+\text{tr}(\mathbf{X}\mathbf{R}_{\mathbf{x}}^{'}\mathbf{X}^{H})) - \text{tr}(\mathbf{R}_{\mathbf{x}}^{'}) + \ \lambda P_{tx}, \tag{2.16a}$$

where λ is the Lagrangian multiplier and

$$\mathbf{X} = \mathbf{K}^{1/2}(\lambda \mathbf{I}_{Nt} - \alpha \mathbf{M})^{-1/2} \tag{2.17}$$

$$\mathbf{K} = \frac{\mathbf{h}\mathbf{h}^{H}}{\sigma_c^2} \tag{2.18}$$

$$\mathbf{M} = \frac{2\gamma_r^{*}\gamma_r}{\sigma_r^2}\dot{\mathbf{A}}^{H}\dot{\mathbf{A}} + \frac{2}{\sigma_r^2}\mathbf{A}^{H}\mathbf{A}, \tag{2.19}$$

and $\mathbf{R}_{\mathbf{x}}$ was substituted by $\mathbf{R}_{\mathbf{x}}^{'}$ as

$$\mathbf{R}_{\mathbf{x}} = (\lambda \mathbf{I}_{Nt} - \alpha \mathbf{M})^{-1/2}\mathbf{R}_{\mathbf{x}}^{'}(\lambda \mathbf{I}_{Nt} - \alpha \mathbf{M})^{-1/2}. \tag{2.20}$$

Based on the singular value decomposition (SVD) of $\mathbf{X} = \mathbf{U}\mathbf{\Sigma}\mathbf{V}^{H}$, it can be shown that the optimizer of P2, $\mathbf{R}_{\mathbf{x}}^{'} = \mathbf{V}\mathbf{P}\mathbf{V}^{H}$, and is shown to be a rank one matrix where $\mathbf{P} = \text{diag}(\epsilon, 0, \cdots, 0)$ is the power of the $\mathbf{R}_{\mathbf{x}}^{'}$. Let us define the Lagrangian function as

$$\mathcal{L} = \frac{(1-\alpha)}{\ln 2}\ln(1+\text{tr}(\mathbf{X}\mathbf{R}_{\mathbf{x}}^{'}\mathbf{X}^{H})) - \text{tr}(\mathbf{R}_{\mathbf{x}}^{'}) + \lambda P_{tx}. \tag{2.21}$$

By substituting $\mathbf{X}, \mathbf{R}_{\mathbf{x}}^{'}$,

$$\mathcal{L} = \frac{(1-\alpha)}{\ln 2}\ln(1+\text{tr}(\mathbf{\Sigma}^2\mathbf{P})) - \text{tr}(\mathbf{P}) + \lambda P_{tx} \tag{2.22}$$

$$\mathcal{L} = \frac{(1-\alpha)}{\ln 2}\ln(1+\epsilon\,\text{tr}(\mathbf{\Sigma}^2)) - \epsilon + \lambda P_{tx}. \tag{2.23}$$

The derivative of the Lagrangian w.r.t. ϵ at the optimum is given as

$$\frac{\partial \mathcal{L}}{\partial \epsilon} = \left(\frac{1-\alpha}{\ln 2}\right)\left(\frac{1}{1+\epsilon\,\text{tr}(\mathbf{\Sigma}^2)}\right)\text{tr}(\mathbf{\Sigma}^2) - 1 = 0 \tag{2.24}$$

$$\epsilon = \left(\frac{1-\alpha}{\ln 2}\right) - \frac{1}{\mathrm{tr}(\mathbf{\Sigma}^2)}. \tag{2.25}$$

Then, we can obtain the optimal solution for the $\mathbf{R}_{\mathbf{x}}^{'}$ and the corresponding closed-form solution up to one scalar (ϵ) for the $\mathbf{R}_{\mathbf{x}}$ in terms of λ are shown in (2.26) and (2.27), respectively.

$$\mathbf{R}_{\mathbf{x}}^{'} = \epsilon \mathbf{v}_1 \mathbf{v}_1^H : \tag{2.26}$$

$$\mathbf{R}_{\mathbf{x}} = \epsilon(\lambda \mathbf{I}_{Nt} - \alpha \mathbf{M})^{-1/2} \mathbf{v}_1 \mathbf{v}_1^H (\lambda \mathbf{I}_{Nt} - \alpha \mathbf{M})^{-1/2}. \tag{2.27}$$

For fixed power P_{tx}, we can find the corresponding Lagrangian variable λ by using any line search method as shown in Fig. 2.2. It can be shown that the above solution satisfies the KKT conditions, which demonstrates the optimally of joint beamforming with the transmit covariance matrix having $\mathrm{rank}(\mathbf{R}_{\mathbf{x}}) = 1$.

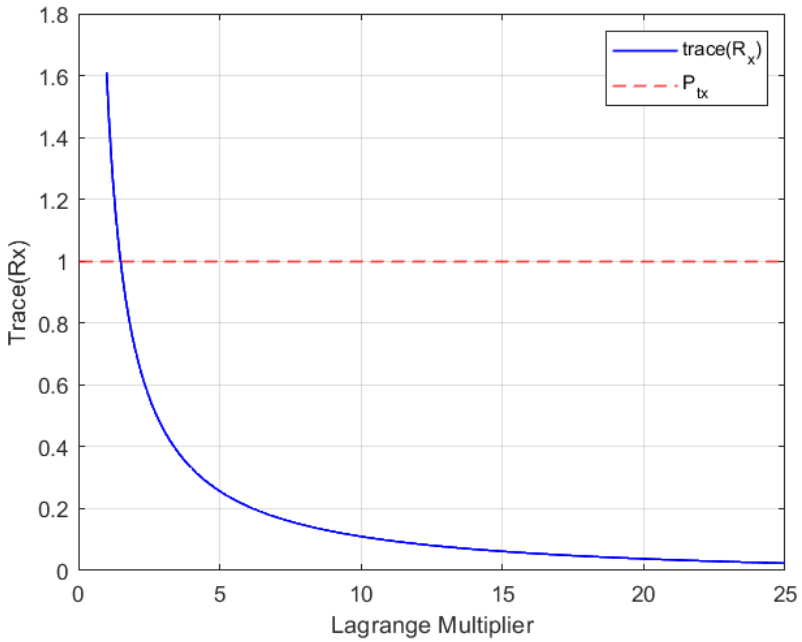


Figure 2.2: Variation of the $\mathrm{tr}(\mathbf{R}_{\mathbf{x}})$ with the Lagrange multiplier.

2.2.3 Proposed Solution - PGD Solution

We adopt the Projected Gradient Descent (PGD) technique to solve the optimization problem. The objective function considered is given by:

$$\mathrm{f} = 2\alpha \,\mathrm{tr}(\mathbf{M}) + \frac{(1-\alpha)}{\log(2)} \left(1 + \mathrm{tr}(\mathbf{K}\mathbf{R}_{\mathbf{x}})\right), \tag{2.28}$$

where $\mathbf{K} = \frac{\mathbf{h}\mathbf{h}^H}{\sigma_c^2}$.

Gradient of the Objective Function

The gradient of the objective function concerning the covariance matrix $\mathbf{R}_{\mathbf{x}}$ is computed as:

$$\frac{\partial \mathrm{f}}{\partial \mathbf{R}_{\mathbf{x}}^T} = 2\alpha \mathbf{M}' + \frac{2(1-\alpha)}{\log(2)} \frac{\mathbf{K}'}{1 + \mathrm{tr}(\mathbf{K}\mathbf{R}_{\mathbf{x}})}. \tag{2.29}$$

Gradient Descent Step

Using the gradient, we update the covariance matrix $\mathbf{R}_{\mathbf{x}}$ with a step-size β as follows:

$$\mathbf{R}_{\mathbf{x}}^{\text{new}} = \mathbf{R}_{\mathbf{x}} + \beta \frac{\partial \mathrm{f}}{\partial \mathbf{R}_{\mathbf{x}}^T}. \tag{2.30}$$

Projection onto the Constraint Set

After the gradient update, the new matrix $\mathbf{R}_{\mathbf{x}}^{\text{new}}$ is projected onto the feasible set. The projection involves finding the matrix $\mathbf{C}$:

$$\mathbf{C} = \mathbf{R}_{\mathbf{x}}^{\text{new}} + \mathbf{E}, \tag{2.31}$$

where $\mathbf{E}$ is the distance between $\mathbf{R}_{\mathbf{x}}^{\text{new}}$ and the projected matrix $\mathbf{C}$.

Projection Optimization Problem

The projection optimization problem is formulated as:

$$\text{P3}: \underset{\mathbf{E}}{\text{minimize}} \quad \frac{1}{2}\|\mathbf{E}\|_F^2 \tag{2.32a}$$

subject to

$$\text{C1}: \text{tr}(\mathbf{R}_{\mathbf{x}}^{\text{new}} + \mathbf{E}) \leq P_{tx}, \tag{2.32b}$$

$$\text{C2}: \mathbf{R}_{\mathbf{x}}^{\text{new}} + \mathbf{E} \succeq 0. \tag{2.32c}$$

Lagrange Relaxation

To solve the projection problem, we apply the Lagrange method. The Lagrangian for the projection optimization problem is:

$$\mathcal{L}(\mathbf{X}, \mu, \mathbf{E}) = \frac{1}{2}\|\mathbf{E}\|_F^2 + \mu\left(\text{tr}(\mathbf{R}_{\mathbf{x}}^{\text{new}} + \mathbf{E}) - P_{tx}\right) - \text{tr}(\mathbf{X}^H(\mathbf{R}_{\mathbf{x}}^{\text{new}} + \mathbf{E})), \tag{2.33}$$

where μ is the Lagrange multiplier, and $\mathbf{X}$ is the Hermitian matrix associated with the constraint $\mathbf{R}_{\mathbf{x}}^{\text{new}} + \mathbf{E} \succeq 0$ ($\mathbf{X} = \mathbf{X}^H$).

The derivative of the Lagrangian with respect to $\mathbf{E}$ is:

$$\frac{\partial \mathcal{L}}{\partial \mathbf{E}} = \mathbf{E} + \mu\mathbf{I} - \mathbf{X}^H = 0, \tag{2.34}$$

which gives the solution for $\mathbf{E}$:

$$\mathbf{E} = \mathbf{X} - \mu\mathbf{I}. \tag{2.35}$$

Lagrange Dual Problem

The dual problem can be formulated as:

$$\text{P4} : \underset{\mu,\mathbf{X}}{\text{maximize}} \quad \mathcal{L}(\mathbf{X}, \mu) \tag{2.36a}$$

subject to

$$\text{C1} : \mu \geq 0, \tag{2.36b}$$

$$\text{C2} : \mathbf{X} \succeq 0. \tag{2.36c}$$

Eigenvalue Decomposition

The solution involves the eigenvalue decomposition (EVD) of the matrices $\mathbf{R}_{\mathbf{x}}^{\text{new}} = \mathbf{U}\Lambda\mathbf{U}^H$ and $\mathbf{X} = \mathbf{U}\Sigma\mathbf{U}^H$, as both matrices share the same eigenbasis. The matrix Σ is determined by:

$$\Sigma = (\mu\mathbf{I} - \Lambda)_+, \tag{2.37}$$

where $(\cdot)_+$ denotes the projection onto the non-negative eigenvalues.

Simplified Lagrange Dual Problem

The dual problem simplifies to:

$$\text{P5} : \underset{\mathbf{E}}{\text{maximize}} \quad -\frac{1}{2}\|\mathbf{R}_{\mathbf{x}}^{\text{new}} - \mu\mathbf{I}\|^2 - \mu P_{tx} + \frac{1}{2}\|\mathbf{R}_{\mathbf{x}}^{\text{new}}\|^2. \tag{2.38}$$

Water-Filling Algorithm

To solve the above problem, we apply the water-filling algorithm. The optimal value for μ is obtained by taking the derivative of the objective function and solving for μ:

$$\mu = \frac{1}{L}\left(\sum_{i=1}^{L}\lambda_i - P_{tx}\right), \tag{2.39}$$

where L is the number of active streams (initialized as $L = N_t$) and the eigenvalues λ_i are sorted in non-increasing order. If the condition $L\lambda_L - \sum_{i=1}^{L} \lambda_i + P_{tx} > 0$ is not satisfied, the number of active streams L is reduced by 1.

The optimal solutions for $\mathbf{E}$ and $\mathbf{C}$ are given by:

$$\mathbf{E} = \mathbf{U}(\Lambda - \mu\mathbf{I})_+\mathbf{U}^H - \mu\mathbf{I}, \tag{2.40}$$

$$\mathbf{C} = \mathbf{U}(\Lambda - \mu\mathbf{I})_+\mathbf{U}^H. \tag{2.41}$$

Computational Complexity

According to the Section 2.2.2, the computational complexity for 2.17 and 2.19 is $\mathcal{O}(N_t^3)$ due to matrix multiplication while 2.18 is $\mathcal{O}(N_t^2)$. For the SVD of 2.17 also have $\mathcal{O}(N_t^3)$ complexity. 2.27 has $\mathcal{O}(N_t^2)$ because matrix vector multiplications. To find the Lagrange multiplier, overall computational complexity $\mathcal{O}(N_t)$. Overall computational complexity for the solution in 2.2.2 is $3\mathcal{O}(N_t^3) + 2\mathcal{O}(N_t^2) + \mathcal{O}(N_t)$ which simplifies to $3\mathcal{O}(N_t^3) + 2\mathcal{O}(N_t^2)$. For Section 2.2.3, according to the **Algorithm**1 for per iteration the overall computational complexity with the dominant operations such as matrix multiplication, EVD is $4\mathcal{O}(N_t^3)$.

Algorithm 1 Projected Gradient Descent Algorithm for Single-user scenario - without EIRP

Inputs: ϵ, P_{tx}, β, $\text{Iter}_{\max}$, $\mathbf{M}$, $\mathbf{K}$

Initialize $\mathbf{R_x}$
Compute $\mathbf{f}_t$
repeat
  Compute Gradient ∇(f) as in 2.29
  repeat
    Compute $\mathbf{R}_x^{t+1}$ as in 2.30
    Compute EVD of $\mathbf{R}_x^{t+1}$ and $\lambda_{\mathbf{NIO}}$
    Initialize $L = N_t$
    repeat
      Compute μ in 2.39
      if $(\lambda_{\mathbf{NIO}}(L) - \mu) \geq 0$ **then**
        $\mu_{optimal} = \mu$
        return $\mu_{optimal}$
      else
        $L = L - 1$
      end if
    until $L \leq N_t$
    Compute $\mathbf{C}$ as in 2.41
    Set $\mathbf{R}_x^{t+1} = \mathbf{C}$
    Compute $\mathbf{f}_{t+1}$
    if $\mathbf{f}_{t+1} \leq \mathbf{f}_t$ **then**
      $\beta = \beta + 1$
    end if
  until $\mathbf{f}_{t+1} \geq \mathbf{f}_t$
until $|\mathbf{E}_{t+1} - \mathbf{E}_t| < \epsilon$

Output: $\mathbf{R}_x$

2.3 Problem Formulation and Solution Approach - With EIRP Limitations

In this section, we examine the impact of EIRP on a JCAS-enabled MIMO system with a single downlink communication user and a single sensing object.

2.3.1 Problem formulation

As in Section 2.2, we similarly define the objective function for this scenario as the weighted sum of the MI and the FI. We can state the optimization problem as follows:

$$\text{P6}: \underset{\mathbf{R_x}}{\text{maximize}} \quad \frac{2\alpha}{\sigma_r^2}\gamma_r^*\gamma_r \,\text{tr}(\dot{\mathbf{A}}\mathbf{R}_x\dot{\mathbf{A}}^H) + \frac{2\alpha}{\sigma_r^2}\,\text{tr}(\mathbf{A}\mathbf{R}_x\mathbf{A}^H) + (1-\alpha)\log_2\left(1+\frac{\mathbf{h}^H\mathbf{R}_x\mathbf{h}}{\sigma_c^2}\right) \tag{2.42a}$$

subject to

$$\text{C1}: \text{tr}(\mathbf{R}_x) \leq P_{tx}, \tag{2.42b}$$

$$\text{C2}: \mathbf{R}_x \preceq \text{EIRP}\ \mathbf{I}, \tag{2.42c}$$

$$\text{C3}: \mathbf{R}_x \succeq 0. \tag{2.42d}$$

Here, the optimization problem is convex due to linearity, and the constraints are convex due to linearity and the positive semi-definiteness of the variable matrix.

2.3.2 Proposed Solution

As a result of the convexity of the optimization problem in (2.42), we can directly use the numerical tool, e.g., MATLAB CVX [59]. However, instead of the numerical tools, we are using other optimization techniques to solve the problem while considering the CVX solution as a reference result to verify the accuracy of the techniques. Here, we mainly focus on the PGD method to solve the problem [60, 61]. The gradient of the

objective function in (2.42) ($\nabla(\mathrm{f}(\mathbf{R_x}))$) using Wirtinger derivatives is as follows:

$$\nabla(\mathrm{f}) = 2\alpha\mathbf{M}^H + 2\frac{(1-\alpha)}{\ln 2}\frac{\mathbf{K}^H}{(1+\mathrm{tr}(\mathbf{K}\mathbf{R}_x))}, \tag{2.43}$$

where $\mathbf{K} = \frac{\mathbf{h}\mathbf{h}^H}{\sigma_c^2}$. The gradient descent step for the covariance matrix $\mathbf{R_x}$ is can be expressed as:

$$\mathbf{R}_x^{\text{new}} = \mathbf{R}_x + \delta\nabla(\mathrm{f}), \tag{2.44}$$

where the δ is the iteration-depend step-size. As the next step of the solution approach, we use an orthogonal projection approach to do the projection onto the constraint set:

$$\mathbf{C} = \mathbf{R}_x^{\text{new}} + \mathbf{E}_o, \tag{2.45}$$

where $\mathbf{E}_o$ is the distance between $\mathbf{C}$ and $\mathbf{R}_x^{\text{new}}$ and it can be found by

$$\mathrm{P7}: \underset{\mathbf{E}}{\text{minimize}} \quad \frac{1}{2}||\mathbf{C} - \mathbf{R}_x^{\text{new}}||_{\mathbf{F}}^2 \tag{2.46a}$$

subject to

$$\mathrm{C1}: \mathrm{tr}(\mathbf{C}) \leq P_{tx}, \tag{2.46b}$$

$$\mathrm{C2}: (\mathrm{EIRP})\mathbf{I} - \mathbf{C} \succeq 0, \tag{2.46c}$$

$$\mathrm{C3}: \mathbf{C} \succeq 0, \tag{2.46d}$$

where $\mathbf{C} = \mathbf{U}\mathbf{\Lambda}\mathbf{U}^H$ and $\mathbf{R}_x^{\text{new}} = \mathbf{U}\mathbf{\Sigma}\mathbf{U}^H$ are the EVD for the problem due to both $\mathbf{C}$ and $\mathbf{R}_x^{\text{new}}$ is in the same eigen basis. Therefore, the simplification of (2.46) is

$$\mathrm{P8}: \underset{\mathbf{E}}{\text{minimize}} \quad \frac{1}{2}||\mathbf{\Lambda} - \mathbf{\Sigma}||_{\mathbf{F}}^2 \tag{2.47a}$$

subject to

$$\mathrm{C1}: \mathrm{tr}(\mathbf{\Lambda}) \leq P_{tx}, \tag{2.47b}$$

$$\mathrm{C2}: \mathbf{0} \leq \mathbf{\Lambda} \leq (\mathrm{EIRP})\mathbf{I}. \tag{2.47c}$$

To solve the problem in (2.47), we can apply the KKT method. The corresponding Lagrange function is:

$$\mathcal{L}_e(\mathbf{X}, \mathbf{Y}, \mathbf{\Lambda}, \mu) = \frac{1}{2}||\mathbf{\Lambda} - \mathbf{\Sigma}||_{\mathbf{F}}^2 + \mu(\text{tr}(\mathbf{\Lambda}) - P_{tx}) + \text{tr}(\mathbf{X}^H(\mathbf{\Lambda} - (\text{EIRP})\mathbf{I})) - \text{tr}(\mathbf{Y}^H\mathbf{\Lambda}), \tag{2.48}$$

where μ is the Lagrangian multiplier and $\mathbf{X}$ and $\mathbf{Y}$ are the hermitian matrix associate with the constraint (2.47c) ($\mathbf{X} = \mathbf{X}^H$ and $\mathbf{Y} = \mathbf{Y}^H$). The derivative w.r.t. $\mathbf{\Lambda}$ is

$$\begin{aligned} \frac{\partial \mathcal{L}_e}{\partial \mathbf{\Lambda}} = \mathbf{\Lambda} - \mathbf{\Sigma} + \mu\mathbf{I} + \mathbf{X} - \mathbf{Y} = 0 \\ \mathbf{\Lambda} = \mathbf{\Sigma} + \mathbf{Y} - \mathbf{X} - \mu\mathbf{I}. \end{aligned} \tag{2.49}$$

The other KKT conditions are in (2.50)-(2.56) which are solved by using an iterative process:

$$\mu(\text{tr}(\mathbf{\Lambda}) - P_{tx}) = 0 \tag{2.50}$$

$$\text{tr}(\mathbf{X}^H(\mathbf{\Lambda} - (\text{EIRP})\mathbf{I})) = 0 \tag{2.51}$$

$$\text{tr}(\mathbf{Y}^H\mathbf{\Lambda}) = 0 \tag{2.52}$$

$$\mu \geq 0 \tag{2.53}$$

$$\text{tr}(\mathbf{\Lambda}) - P_{tx} \leq 0 \tag{2.54}$$

$$\mathbf{X}, \mathbf{Y} \succeq 0 \tag{2.55}$$

$$0 \leq \mathbf{\Lambda} \leq (\text{EIRP})\mathbf{I}. \tag{2.56}$$

We present the overall algorithm in **Algorithm 2**. The algorithm runs until the stopping criteria as in (2.57) is satisfied with $\epsilon \in \mathbb{R}_+$ and the maximum number of iterations Iter_{max} is reached:

$$\mathbf{E}_t = \quad \alpha\,\text{tr}(\mathbf{M}\mathbf{R}_x^t) + \frac{(1-\alpha)}{\ln 2}\ln\left|1 + \text{tr}(\mathbf{K}\mathbf{R}_x^t)\right|. \tag{2.57}$$

Algorithm 2 Projected Gradient Descent Algorithm for Single-user scenario - with EIRP

Inputs: ϵ, P_{tx}, δ, $\text{Iter}_{\max}$, $\mathbf{M}$, $\mathbf{K}$

1: Initialize $\mathbf{R}_{\mathbf{x}}^{0}$
2: $\mathbf{R}_{x}^{\text{t}} = \mathbf{R}_{x}^{0}$
3: Compute $\mathbf{E}_t$
4: **repeat**
5: Compute Gradient ∇(f) as in 2.43
6: Compute $\mathbf{R}_{x}^{t+1} = \mathbf{R}_{\mathbf{x}}^{t} + \beta\nabla$(f)
7: Compute $\mathbf{R}_{x}^{t+1} = \mathbf{U}\boldsymbol{\Sigma}\mathbf{U}^{H}$
8: Set $\boldsymbol{\Sigma}$ into non-increasing order
9: $\boldsymbol{\Lambda}^{'} \leftarrow$ Output of the projection
10: Compute $\mathbf{R}_{x}^{\text{proj}} = \mathbf{U}\boldsymbol{\Lambda}^{'}\mathbf{U}^{H}$
11: Set $\mathbf{R}_{x}^{t+1} = \mathbf{R}_{x}^{\text{proj}}$
12: Set $\mathbf{E}_t = \mathbf{E}_{t+1}$
13: **until** $|\mathbf{E}_{t+1} - \mathbf{E}_t| < \epsilon$
14: **return** $\mathbf{R}_x$

2.3.3 Analysis of Computational Complexity

Consider the optimization algorithm presented in **Algorithm 2**. The complexity for computing $\mathbf{M}$ (as outlined in (2.19)) and $\mathbf{K}$ (as described in (2.43)) is $\mathcal{O}(N_t^3)$ and $\mathcal{O}(N_t^2)$, respectively, due to the operations involved, such as matrix-matrix multiplication and the vector outer product. Similarly, determining ∇(f) and $\mathbf{R}_x^{t+1}$ also incurs a complexity of $\mathcal{O}(N_t^3)$ as these calculations involve matrix-matrix multiplications. The EVD of $\mathbf{R}_x^{t+1}$ has a computational complexity of $\mathcal{O}(N_t^3)$. In the projection step, solving the problem using the KKT conditions results in an overall complexity of $\mathcal{O}(N_t^3)$. The calculation of $\mathbf{R}_x^{\text{proj}}$ also requires $\mathcal{O}(N_t^3)$ in terms of computational resources. As a result, the

overall computational complexity of the algorithm is $7\mathcal{O}(N_t^3) + \mathcal{O}(N_t^2)$, which simplifies to $7\mathcal{O}(N_t^3)$.

2.4 Simulation Results

This section presents and analyzes the numerical results obtained for the case of single-user communication without and with EIRP limitations.

2.4.1 Simulation Parameters

For all the results, the parametric channel model [62], [63] is considered for the downlink users in the simulations. Parametric channel modeling with array response vectors provides an efficient framework for modern wireless systems like massive MIMO and mmWave communications by representing channels through geometric parameters (AoA, AoD, path gains) rather than full channel matrices. This approach reduces computational overhead while maintaining physical interpretability, enabling precise beamforming through phase-aligned array responses. Particularly effective in sparse, directional propagation environments, it leverages the inherent structure of high-frequency channels for scalable massive MIMO implementations. While limited in richly scattered scenarios, its integration with data-driven methods offers promising extensions for complex real-world deployments, making it fundamental for 5G/6G systems and beyond.

Moreover, P_{Loss} is the distance depends on path loss, and it is given by

$$P_{Loss} = \quad \mathrm{P}_0 \left(\frac{d}{d_0} \right)^{\eta}, \tag{2.58}$$

where d_0 is the reference distance and η is the path loss exponent. Set the parameters as follows: $P_{tx} = 30$ dBm, $\sigma_c^2 = \sigma_r^2 = 0$ dBm, $d_0 = 1$ m, $\eta = 3.2$, P_0 is the path loss at d_0 and the weighting parameter (α) is selected due to the prioritization between

communication and sensing and we determined the α is varied in the range of [0,1]. We assume the sensing object to be at 0°. In our simulations, we vary the AoD for the communication user and the number of transmitting and receiving antennas at the BS. Moreover, for the communication users we consider 6 NLOS paths.

2.4.2 Without EIRP Limitations

Shared Beamforming for Optimal JCAS

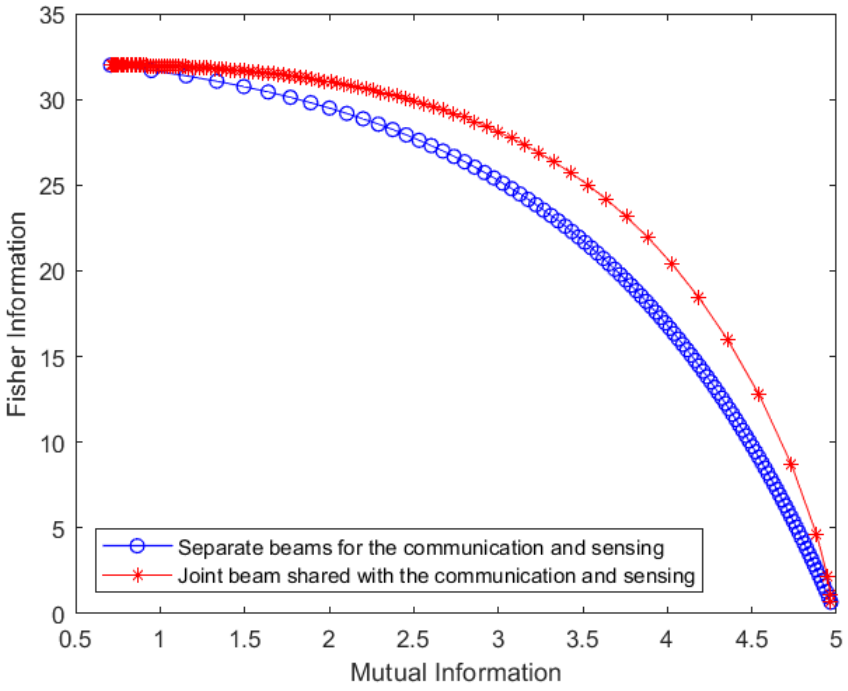


Figure 2.3: Comparison between joint and separate beamforming for communication and sensing in terms of the trade-off between mutual information and Fisher information.

JCAS can be achieved in two ways: (i) The two functions are physically part of one system, but they employ separate beamforming for communication and sensing; (ii)

Joint beamforming is used which needs to be optimized for both communication and sensing performances [64]. In case (i), the total transmit power at the BS is split between these two independent beams and two beamforming matrices for communication ($\mathbf{R}_{\mathbf{x}_{\mathbf{MI}}} \in \mathbb{C}^{N_t \times N_t}$) and sensing ($\mathbf{R}_{\mathbf{x}_{\mathbf{FI}}} \in \mathbb{C}^{N_t \times N_t}$) have to be optimized separately. We can express the beamforming matrix; $\mathbf{R}_{\mathbf{x}_{\mathbf{T}}}$ for this scenario using the parameter α, as follows:

$$\mathbf{R}_{\mathbf{x}_{\mathbf{T}}} = \alpha \mathbf{R}_{\mathbf{x}_{\mathbf{FI}}} + (1-\alpha)\mathbf{R}_{\mathbf{x}_{\mathbf{MI}}}. \tag{2.59}$$

However, as mentioned in Section 2.2, the joint beamforming matrix (see (2.27)), $\text{rank}(\mathbf{R}_{\mathbf{x}}) = 1$ because there is only one beamforming vector for both functions as opposed to the separate beamforming with $\text{rank}(\mathbf{R}_{\mathbf{x}_{\mathbf{T}}}) = 2$. Fig. 2.3 illustrates that joint beamforming is the optimal approach for JCAS with better performance. Moreover, the trade-off indicates that when $\alpha = 0$, the beam is directed towards the communication user and when $\alpha = 1$, the beam is directed towards the sensing target because the MI content and the FI content are higher, respectively.

Verification of the Closed-form Solution

From this point onward, we focus on designing the joint beamforming matrix and validating the accuracy of the closed-form solution. It is essential to demonstrate that the derived closed-form expression achieves a level of precision comparable to the numerical solution obtained using convex optimization techniques. The results presented in Fig. 2.4 confirm a strong agreement between the closed-form solution and the corresponding numerical results from the CVX toolbox, thereby validating the accuracy of our analytical approach. Furthermore, we examine the robustness of the closed-form solution by analyzing its validity under different system configurations, particularly varying numbers of N_t and N_r. Our findings indicate that the closed-form solution remains consistent across different values of N_t and N_r, reinforcing its general applica-

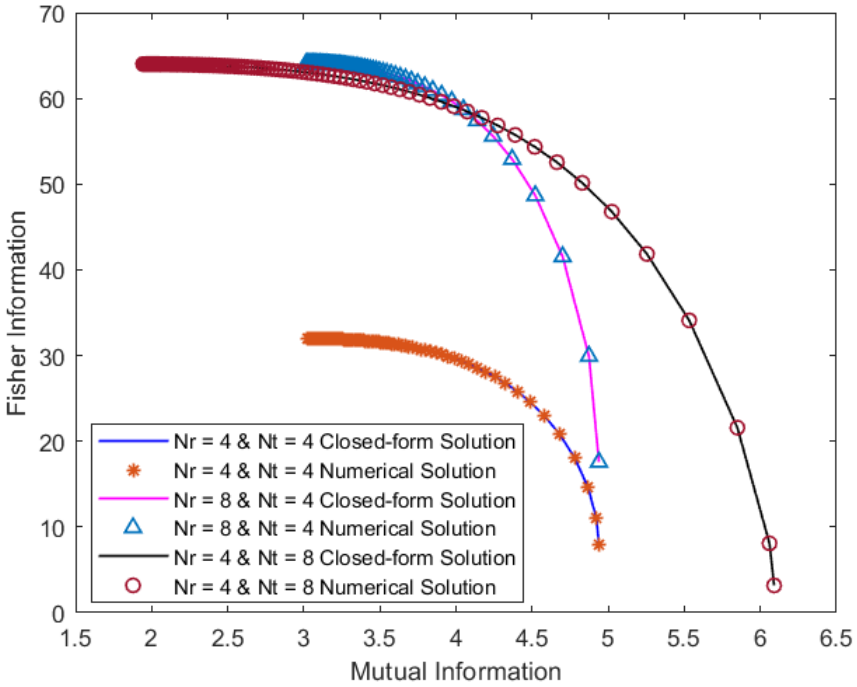


Figure 2.4: Closed-form rank-one solution and numerical (using CVX toolbox) solution for different values of N_r and N_t.

bility. A detailed discussion of the impact of these variations on system performance will be provided in subsequent sections.

Verification of PGD Solution

This section validates the accuracy and efficiency of the PGD optimization technique, as discussed in Section 2.2.3, by comparing its results with numerical solutions obtained from the CVX toolbox. Figure 2.5 demonstrates a strong correlation between both methods, confirming the correctness and reliability of PGD. This consistency underscores PGD's computational efficiency, positioning it as a viable alternative to convex solvers such as CVX, which are often more computationally demanding.

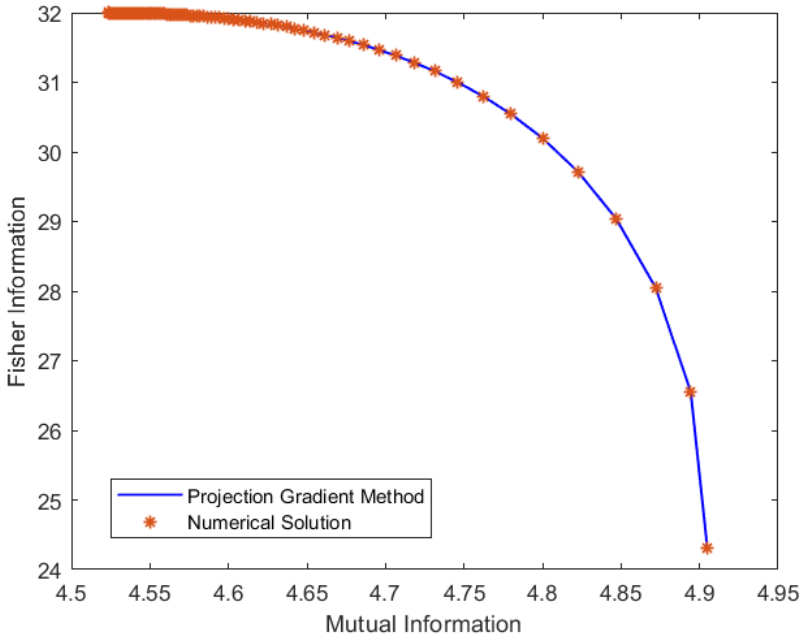


Figure 2.5: PGD solution and numerical (using CVX toolbox) solution.

Effect of Angle of Departure

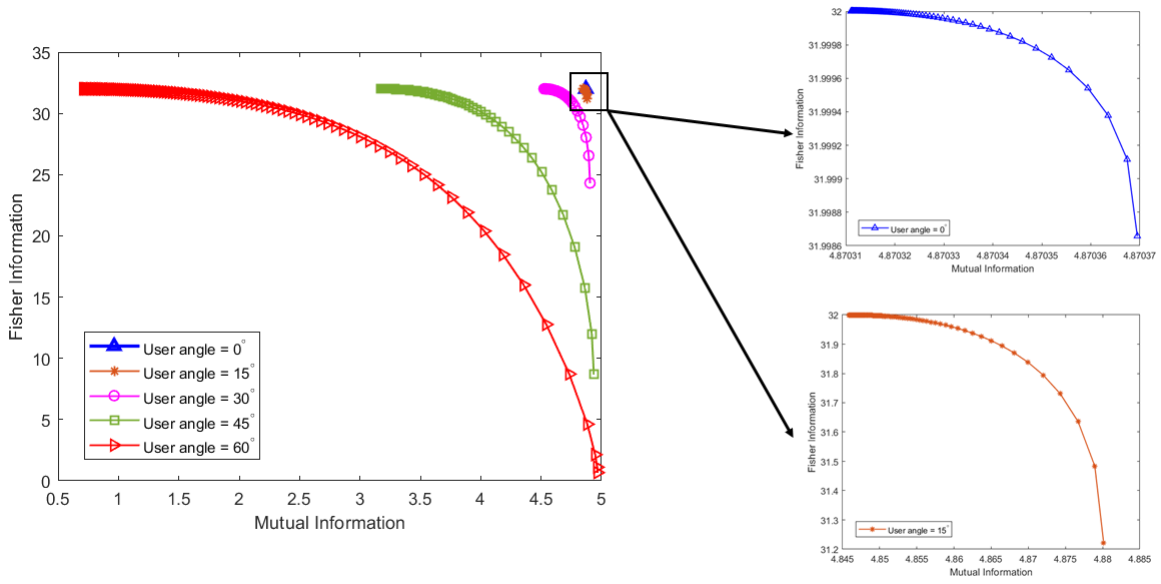
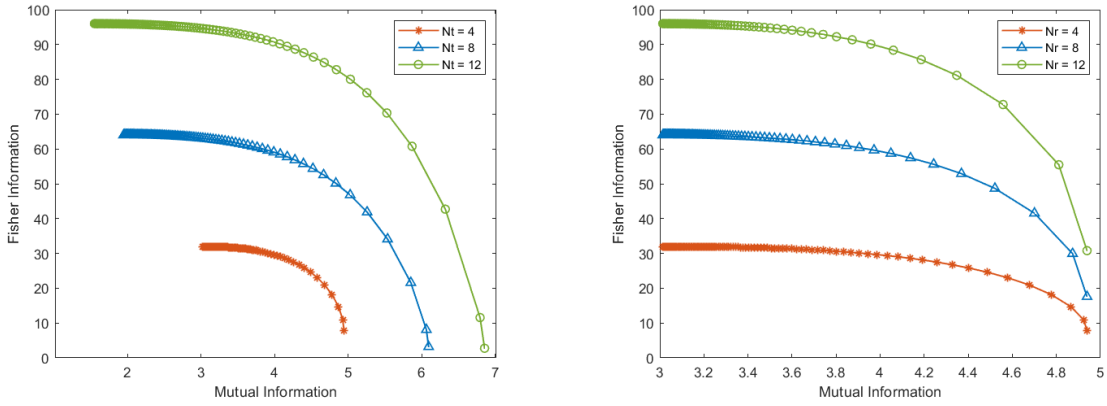


Figure 2.6: Variation of the trade-off with AoD of the user with $N_r = 4$ and $N_t = 4$.

Consider the line-of-sight case for the communication user, with $\mathbf{h}^H \propto \mathbf{a}^T(\theta_c)$, as in (2.12), where θ_c represents the AoD corresponding to the communication user. Fig. 2.6 shows how the trade-off varies with θ_c when θ_r is fixed. If the user and the sensing object are placed at the same location, the total transmit power is directed to it, and intuitively, we can say that there is no trade-off. Therefore, the MI and the FI are not severely competing goals (see zoomed-in figures of Fig. 2.6), making the trade-off negligible. As θ_c increases, the beamformer must be optimized for both the communication user and the sensing object, and the trade-off becomes noticeable. To achieve better performance in both communication and sensing while enhancing overall system performance, it is better to have the user and target in similar directions.

Effect of the Number of Transmitting and Receiving Antennas



(a) $N_t \geq N_r$ (b) $N_t \leq N_r$

Figure 2.7: Variation of the trade-off with (a) the number of transmitting antennas, (b) the number of receiving antennas.

Next, we analyze the variation of the trade-off with N_r and N_t. Here, we can consider two cases:

- Case I: Number of transmitting antennas greater than or equal to the number of

receiving antennas ($N_t \geq N_r$).

- Case II: Number of transmitting antennas less than or equal to the number of receiving antennas ($N_t \leq N_r$).

Fig. 2.7 illustrates the interpretation of Case I and Case II, respectively. The number of transmitting antennas affects both communication (as seen in (2.2)) and sensing (as demonstrated in (2.3) and (2.4)) performances. As shown in Fig. 2.7(a), when the value of N_t increases, the ranges of variation for both the MI and the FI increase. Therefore, to enhance both communication and sensing performances, it is advisable to increase the number of transmitting antennas.

According to Fig. 2.7(b), we can observe that only FI increases as N_r increases, as expected. In fact, for the downlink communication in (2.2), the communication user's performance depends entirely on N_t. Therefore, the MI approaches a constant range, while the sensing performance is enhanced. Therefore, if our focus is totally on the sensing side, it is better to consider case II and deploy a high number of receiving antennas.

2.4.3 With EIRP Limitations

We consider $Nr = Nt = 4, 8$ with a single communication user and sensing object. Furthermore, we change the EIRP value from 27.78 dBm to 29.54 dBm (i.e., from 0.6 W to 0.9 W).

Verification of PGD Solution

According to Fig. 2.8, for EIRP is 27.78 dBm, shows the proposed optimization algorithm (see **Algorithm 2**) provides results similar to those from the numerical tool (i.e., MATLAB CVX). Moreover, we observe the behavior of the trade-off with the number

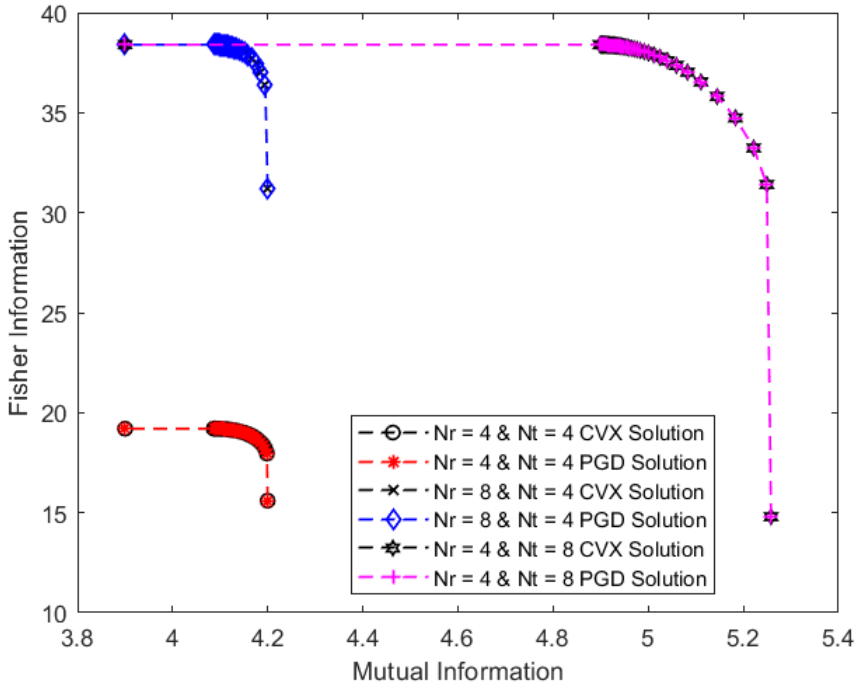


Figure 2.8: Comparison between numerical and PGD solutions for different N_r and N_t values.

of transmitting and receiving antenna variations in this EIRP scenario. When we increase the N_r, the sensing performances increase while the communication performances vary in a fixed range. On the other hand, when we increase N_t, it has a fixed sensing performance range while the communication performance increases.

Variation of the Trade-off With EIRP Values with closer user and sensing object

We illustrate the behavior of the trade-off between communication and sensing with varying EIRP values. Fig. 2.9 depicts this trade-off for various EIRP values. According to this figure, sensing and communication performances improve as the EIRP value increases. Furthermore, when the EIRP decreases, the points for $\alpha = 0$ and $\alpha = 1$ move

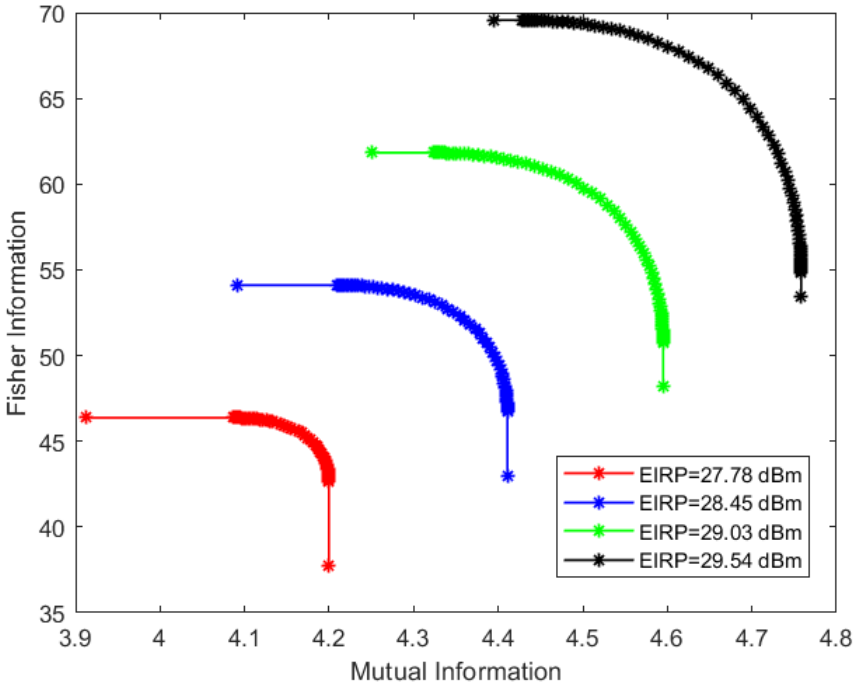


Figure 2.9: Comparison between the communication and sensing performance trade-off with EIRP values user at $\pi/6$.

away from the trade-off in the vertical and horizontal directions, respectively.

When $\alpha = 0$, the optimization problem focuses on MI, and theoretically, FI should be zero. Conversely, when $\alpha = 1$, the focus is on FI, and MI should theoretically be zero. However, neither MI nor FI becomes zero when we optimize MI and FI in these two scenarios. Instead, they stabilize at specific values concerning the threshold value. Thus, for the cases of $\alpha = 0$ and $\alpha = 1$, FI and MI values can be placed between these vertical and horizontal straight lines. In conclusion, as EIRP decreases, the best trade-off is the curve within the $0 \leq \alpha \leq 1$.

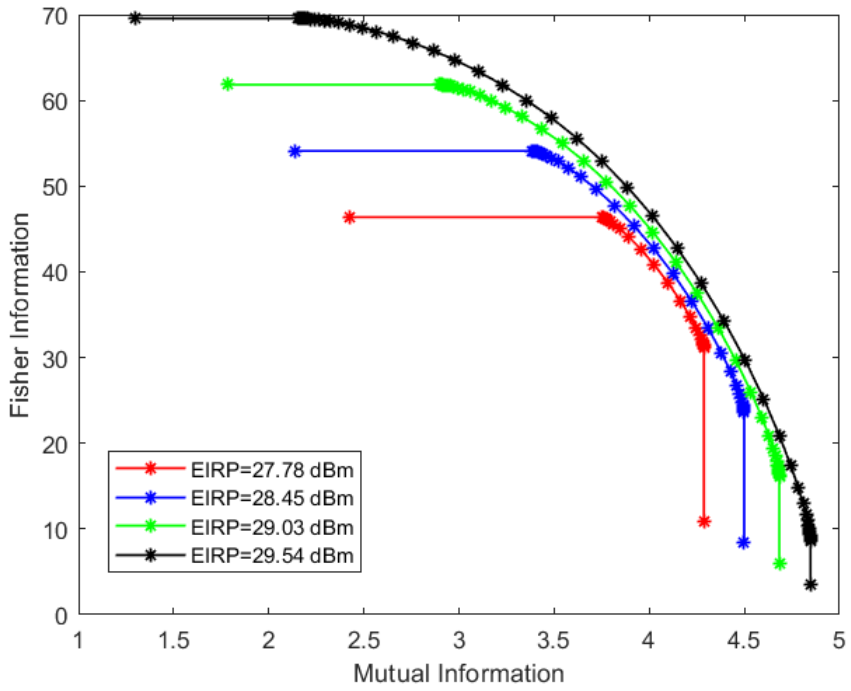


Figure 2.10: Comparison between the communication and sensing performance trade-off with EIRP values user at $\pi/2$.

Variation of the Trade-off With EIRP Values with far user and sensing object

In Fig. 2.10, we illustrate the deviation of the trade-off when the user is away from the sensing object. Here, we placed the downlink user at the $\pi/2$ position. According to the figure, we observe high information degradation when $\alpha = 0$ and $\alpha = 1$, while degradation is lower in the $0 < \alpha < 1$ range. Therefore, we conclude that when the system operates in the joint communication and sensing region, the impact of the EIRP constraint is smaller because the total power at the BS is shared between two beams, reducing the EIRP.

2.5 Chapter Summary

This chapter presented a comprehensive system model and analysis for a JCAS-enabled MIMO BS equipped with separate transmitting and receiving antenna arrays. The system model considered a single downlink communication user and a sensing object, such as a UAV, with assumptions that LOS and NLOS conditions affect communication, while only LOS impacts sensing. The signal model for both downlink communication and sensing echo signals was derived, incorporating beamforming vectors, channel responses, and noise models.

The chapter formulated a multi-objective optimization problem to maximize the weighted sum of MI for the communication user and FI for the sensing object under a total power constraint. Two solution approaches were proposed: a closed-form solution using Lagrange optimization and a PGD method. The closed-form solution was validated against numerical results from the CVX toolbox, demonstrating its accuracy and robustness across different system configurations. The PGD method was also verified, showing strong agreement with CVX results and highlighting its computational efficiency.

Key findings from the simulations include:

- **Joint vs. Separate Beamforming:** Joint beamforming outperforms separate beamforming for communication and sensing, achieving better trade-offs between MI and FI.

- **Impact of AoD:** The trade-off between MI and FI becomes more pronounced as the AoD of the communication user increases relative to the sensing object. When the user and sensing object are co-located, the trade-off is negligible.

- **Antenna Configuration:** Increasing the number of transmitting antennas enhances both communication and sensing performances, while increasing the num-

ber of receiving antennas primarily improves sensing performance.

- **EIRP Limitations:** The trade-off between MI and FI is influenced by EIRP constraints. As EIRP decreases, the trade-off curve shifts, and the system performance stabilizes at specific threshold values for MI and FI.

The chapter concludes that joint beamforming is the optimal strategy for JCAS systems, particularly when the communication user and sensing object are in similar directions. The proposed closed-form and PGD solutions provide efficient and accurate methods for optimizing beamforming in JCAS-enabled MIMO systems, even under EIRP constraints. These findings lay the groundwork for further exploration of multi-user scenarios and advanced optimization techniques in subsequent chapters.

Chapter 3

Characterizing the Pareto Boundary for JCAS in a Multi-User MIMO System

3.1 System Model and Assumptions

We consider a JCAS-enabled MIMO BS equipped with two separate antenna arrays: N_t transmitting antennas and N_r receiving antennas. As shown in Fig. 3.1, the MIMO BC system model includes K single-antenna downlink users (where $K < N_t$) and a sensing object. We assume that line-of-sight (LOS) and non-line-of-sight (NLOS) conditions affect downlink communication, while only LOS affects sensing.

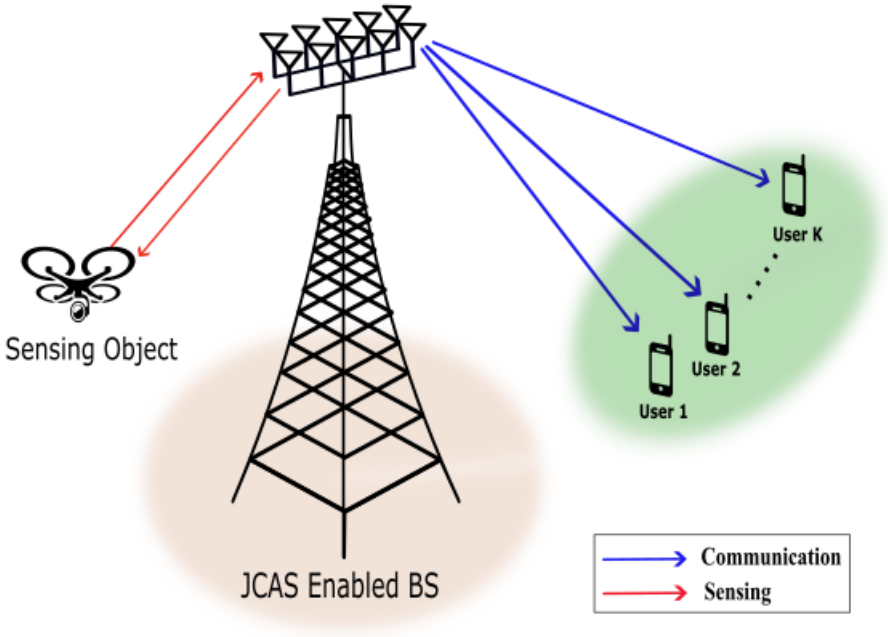


Figure 3.1: Joint communication and sensing model of MIMO BC.

3.1.1 Signal Model

As shown in the MIMO BC system model (Fig. 3.1), we represent the JCAS signal from the BS as $\mathbf{x}_{BC} \in \mathbb{C}^{N_t}$:

$$\mathbf{R}_x = \mathbb{E}[\mathbf{x}_{BC}\mathbf{x}_{BC}^H] = \sum_{i=0}^{K} \mathbf{w}_i \mathbf{w}_i^H, \tag{3.1}$$

where $\mathbf{w}_i \in \mathbb{C}^{N_t}$ is the beamforming vector for the i^{th} downlink user.

We define the JCAS downlink covariance matrices $\mathbf{R}_i \in \mathbb{C}^{N_t \times N_t}$ for $i = 1,...,K$ with the total power constraint $\sum_{i=1}^{K} \text{tr}(\mathbf{R}_i) \leq P_{tx}$, where P_{tx} is the transmit power budget. The received signal by the communication users of the MIMO BC is,

$$y_i = \mathbf{h}_i^H \mathbf{x}_{BC} + z_i, \tag{3.2}$$

in which $\mathbf{h}_i^H \in \mathbb{C}^{1 \times N_t}$ is the downlink channel vector of the i^{th} user. The random variable z_i is the AWGN with zero mean and σ_c^2 variance.

Let us consider the MIMO MAC system model for the user side of Fig. 3.1. The JCAS signal to the BS from the uplink users is represented as $x_i \in \mathbb{C}$. We define the uplink covariance matrices $Q_i \in \mathbb{C}$ with the total power constraint of $\sum_{i=1}^{K} \mathrm{tr}(Q_i) \leq P_{tx}$. The received signal at the BS from users of the MIMO MAC is,

$$\mathbf{y}_{MAC} = \sum_{i=1}^{K} \mathbf{h}_i x_i + \mathbf{z}, \tag{3.3}$$

where $\mathbf{h}_i$ is the dual uplink channel vector for the i^{th} user and $\mathbf{z}$ is the AWGN with zero mean and σ_c^2 variance for all elements.

On the sensing side, the BS transmits $\mathbf{x}_{BC}$ to the sensing object, and the BS receives the reflected echo signal

$$\mathbf{y}_r = \mathbf{G}\mathbf{x}_{BC} + \mathbf{z}_r, \tag{3.4}$$

where $\mathbf{z}_r \in \mathbb{C}^{N_r}$ is the AWGN with zero mean and σ_r^2 variance for each. $\mathbf{G} \in \mathbb{C}^{N_r \times N_t}$ denotes the target response matrix, and for a single target case, it can be represented as:

$$\mathbf{G} = \gamma_r \mathbf{b}(\theta_r)\mathbf{a}^T(\theta_r), \tag{3.5}$$

with

$$\mathbf{a}\left(\theta_r\right) = \left[e^{-j\frac{N_t-1}{2}k\sin\theta_r}, e^{-j\frac{N_t-3}{2}k\sin\theta_r}, \ldots, e^{j\frac{N_t-1}{2}k\sin\theta_r}\right]^T, \tag{3.6}$$

where $\gamma_r \in \mathbb{C}$ is the reflection coefficient which includes both radar cross-section and round trip path-loss, and θ_r is the angle of the sensing object relative to the BS and where $k = \frac{2\pi d}{\lambda}$, d is the distance between two adjacent antennas in the array, λ is the wavelength. The vector $\mathbf{a}(\theta_r) \in \mathbb{C}^{N_t}$ (as given in (3.6)) denotes the transmit array response vector assuming that the antenna array has its origin located at the center. Similarly, we can express $\mathbf{b}(\theta_r) \in \mathbb{C}^{N_r}$, which is the receive array response vector. In our case, the AoA and AoD are equal (i.e., a monostatic radar).

3.1.2 MI for the Communication User

In [60,65–67], the sum-rate capacity of the MIMO BC (denoted as C_{BC}) can be achieved by the dirty paper coding [68]. Then, the sum-rate capacity of the MIMO BC can be expressed in terms of maximization with the power constraint $\sum_{i=1}^{K} \mathrm{tr}(\mathbf{R}_i) \leq P_{tx}$ as follows:

$$C_{BC} = \max_{\{\mathbf{R}_i\}_{i=1}^{K}} \sum_{i=1}^{K} \log \frac{\left|1 + \mathbf{h}_i^H (\sum_{j=1}^{i} \mathbf{R}_j) \mathbf{h}_i\right|}{\left|1 + \mathbf{h}_i^H (\sum_{j=1}^{i-1} \mathbf{R}_j) \mathbf{h}_i\right|}. \tag{3.7}$$

We observe that (3.7) is not a concave function. Therefore, the optimization problem concerning $\mathbf{R}_i$ is nontrivial. However, with the duality of the uplink and downlink established in the dirty paper region, the MIMO capacity, C_{BC} is equal to the MIMO MAC capacity (C_{MAC}) [65, 69]:

$$C_{BC}(\mathbf{h}_1^H, ..., \mathbf{h}_K^H, P_{tx}) = C_{MAC}(\mathbf{h}_1, ..., \mathbf{h}_K, P_{tx}). \tag{3.8}$$

The sum-rate capacity of the MIMO MAC with the power constraint of $\sum_{i=1}^{K} \mathrm{tr}(Q_i) \leq P_{tx}$ is

$$C_{MAC} = \max_{\{Q_i\}_{i=1}^{K}} \log_2 \left| \mathbf{I} + \sum_{i=1}^{K} \mathbf{h}_i Q_i \mathbf{h}_i^H \right|. \tag{3.9}$$

We can rewrite the C_{MAC} as follows:

$$\begin{aligned} C_{MAC} &= \log_2 \left| \mathbf{I} + \sum_{j \neq 1}^{K} \mathbf{h}_j Q_j \mathbf{h}_j^H + \mathbf{h_i} Q_i \mathbf{h}_i^H \right| \\ &= \log_2 \left| \mathbf{A}_M^{1/2} \left(\mathbf{I} + \mathbf{A}_M^{-1/2} \mathbf{B}_M \mathbf{A}_M^{-1/2} \right) \mathbf{A}_M^{1/2} \right| \\ &= \log_2 \left| \mathbf{A}_M \left(\mathbf{I} + \mathbf{A}_M^{-1/2} \mathbf{B}_M \mathbf{A}_M^{-1/2} \right) \right| \\ &= \log_2 |\mathbf{A}_M| + \log_2 \left| \mathbf{I} + \mathbf{A}_M^{-1/2} \mathbf{B}_M \mathbf{A}_M^{-1/2} \right|, \end{aligned} \tag{3.10}$$

where $\mathbf{A}_M = \mathbf{I} + \sum_{j \neq 1}^{K} \mathbf{h}_j Q_j \mathbf{h}_j^H$ and $\mathbf{B}_M = \mathbf{h}_i Q_i \mathbf{h}_i^H$. (3.10) is equivalent to the capacity of point-to-point MIMO channel with effective channel of $\mathbf{h}_{ei}^H = \mathbf{h}_i^H \mathbf{A}_M^{-1/2}$ with the power

constraint of $\text{tr}(Q_i) \leq P_i$ [65].

$$C_{MAC} = \max_{\{Q_i\}_{i=1}^{K}:\sum_{i=1}^{K}\text{tr}(Q_i)\leq P_{tx}} \sum_{i=1}^{K} \log_2 \left|\mathbf{I} + \mathbf{h}_{ei} Q_i \mathbf{h}_{ei}^H\right|. \tag{3.11}$$

Treating these $\mathbf{he}_i$ effective channels as parallel and non-interfering, we can obtain the sum-rate capacity as in (3.11).

3.1.3 FI for Sensing Object

With the observation model in (3.4), the BS knows $\mathbf{x}_{BC}$, and using the estimating vector $\mathbf{v} = [\theta_r \quad \gamma_r \quad \gamma_r^*]^T$, we can express the FI matrix, $\mathbf{J}_i$, along with each user (see **Appendix A**):

$$\mathbf{J}_i = \frac{1}{\sigma_r^2} \begin{bmatrix} J_{(1,1)} & J_{(1,2)} & J_{(1,3)} \\ J_{2,1)} & J_{(2,2)} & 0 \\ J_{(3,1)} & 0 & J_{(3,3)} \end{bmatrix}, \tag{3.12}$$

with

$$J_{(1,1)} = 2\gamma_r^* \gamma_r \,\text{tr}(\dot{\mathbf{A}}\mathbf{R}_i \dot{\mathbf{A}}^H) \tag{3.13}$$

$$J_{(2,2)} = \text{tr}(\mathbf{A}\mathbf{R}_i \mathbf{A}^H) \tag{3.14}$$

$$J_{(3,3)} = \text{tr}(\mathbf{A}\mathbf{R}_i \mathbf{A}^H) \tag{3.15}$$

$$J_{(1,2)} = J_{(2,1)} = \gamma_r^* \,\text{tr}(\mathbf{A}\mathbf{R}_i \dot{\mathbf{A}}^H) \tag{3.16}$$

$$J_{(1,3)} = J_{(3,1)} = \gamma_r \,\text{tr}(\dot{\mathbf{A}}\mathbf{R}_i \mathbf{A}^H), \tag{3.17}$$

where $\dot{\mathbf{A}} = \frac{\partial \mathbf{A}}{\partial \theta_r}$ and $\mathbf{A} = \mathbf{b}(\theta_r)\mathbf{a}^T(\theta_r)$. The derivative of the transmit array response vector is mentioned in (3.18); similarly, we can write the derivative of the receive array response vector.

$$\dot{\mathbf{a}}\,(\theta_r) = \left[-ja_1 \frac{N_t - 1}{2} k \cos\theta_r, \ldots, -ja_{N_t} \frac{N_t - 1}{2} k \cos\theta_r\right]^T, \tag{3.18}$$

Regarding the sensing performance metric, we use the trace of the FI matrix due to its mathematical tractability. We are motivated by our observation that the parameters γ_r and θ_r do not strongly couple, and the FI matrix remains mainly diagonal. Therefore, we consider the trace of $\mathbf{J}$ as follows:

$$\mathrm{tr}(\mathbf{J}) = \frac{2}{\sigma_r^2}(\gamma_r^* \gamma_r \,\mathrm{tr}(\dot{\mathbf{A}}\mathbf{R}_x\dot{\mathbf{A}}^H) + \mathrm{tr}(\mathbf{A}\mathbf{R}_x\mathbf{A}^H)), \tag{3.19}$$

where $\mathbf{R}_x = \sum_{i=1}^{K} \mathbf{w}_i\mathbf{w}_i^H + \mathbf{w}_0\mathbf{w}_0^H = \sum_{i=1}^{K} \mathbf{R}_i + \mathbf{R}_0$ with the $\mathbf{w}_0$ is the beamforming vector for the sensing object. Using the properties of trace, we can simplify the (3.19) as follows:

$$\mathrm{tr}(\mathbf{J}) = \mathrm{tr}\left(\mathbf{M}\left(\sum_{i=1}^{K} \mathbf{R}_i + \mathbf{R}_0\right)\right) \tag{3.20}$$

where $\mathbf{M} = \frac{2\gamma_r^*\gamma_r}{\sigma_r^2}\dot{\mathbf{A}}^H\dot{\mathbf{A}} + \frac{2}{\sigma_r^2}\mathbf{A}^H\mathbf{A}$.

3.2 Problem Formulation

Based on (3.7) and (3.20), we formulate a multi-objective optimization problem. Moreover, in this part, we try to apply the BC to MAC transformation for further simplifications. Our main objective is to maximize the weighted sum of the MI (sum-rate capacity) and the FI under the power budget constraint. The problem formulation for

the MIMO BC is as follows:

$$\begin{aligned}\text{P1}: \underset{\{\mathbf{R}_i\}_{i=1}^{K},\mathbf{R}_0}{\text{maximize}} \quad & \alpha \operatorname{tr}\left(\mathbf{M}\left(\sum_{i=1}^{K}\mathbf{R}_i+\mathbf{R}_0\right)\right) \\ & +(1-\alpha)\sum_{i=1}^{K}\log\frac{\left|1+\mathbf{h}_i^H(\sum_{j=1}^{i}\mathbf{R}_j)\mathbf{h}_i\right|}{\left|1+\mathbf{h}_i^H(\sum_{j=1}^{i-1}\mathbf{R}_j)\mathbf{h}_i\right|} \qquad (3.21a)\end{aligned}$$

subject to

$$\text{C1}: \sum_{i=1}^{K}\operatorname{tr}(\mathbf{R}_i)+\operatorname{tr}(\mathbf{R}_0)\le P_{tx}, \qquad (3.21b)$$

$$\text{C2}: \mathbf{R}_i \succeq 0, \quad \forall i=1,\ldots,K, \qquad (3.21c)$$

$$\text{C3}: \mathbf{R}_0 \succeq 0. \qquad (3.21d)$$

The optimization problem in (3.21) is a non-convex optimization problem for $K \geq 2$ due to the ratio of the (3.7). Therefore, we use the dual uplink transformation for communication users. Then, the new optimization problem is as follows:

$$\begin{aligned}\text{P2}: \underset{\{Q_i\}_{i=1}^{K},\mathbf{R}_0}{\text{maximize}} \quad & \alpha\sum_{i=1}^{K}\operatorname{tr}(\mathbf{M}\mathbf{c}_i Q_i \mathbf{c}_i^H)+\alpha\operatorname{tr}(\mathbf{M}\mathbf{R}_0) \\ & +(1-\alpha)\sum_{i=1}^{K}\log_2\left|\mathbf{I}+\mathbf{h}_{ei}Q_i\mathbf{h}_{ei}^H\right| \qquad (3.22a)\end{aligned}$$

subject to

$$\text{C1}: \sum_{i=1}^{K}Q_i+\mathbf{R}_0\le P_{tx}, \qquad (3.22b)$$

$$\text{C2}: Q_i \geq 0; \quad \forall i=1,...,K, \qquad (3.22c)$$

$$\text{C3}: \mathbf{R}_0 \succeq 0, \qquad (3.22d)$$

where $0 \leq \alpha \leq 1$ is the weighted value.

Proposition 3.1: With the condition of independently distributed of channels, a candidate optimal solution of (3.22) satisfies:

Case 01: $0 \leq \alpha < 1$, $\texttt{rank}(Q_i) = 1$, $\forall i \in (1, .., K)$ and $\texttt{rank}(\mathbf{R}_0) = 0$.

Case 02: $\alpha = 1$, there is no distinction between Q_i or $\mathbf{R}_0$. The optimal solution may allocate power to Q_i or $\mathbf{R}_0$ interchangeably.

Proof: See **Appendix B**.

In our optimization problem, the objective function consists of two terms. The first term,

$$\alpha \sum_{i=1}^{K} \text{tr}(\mathbf{M}\mathbf{c}_i Q_i \mathbf{c}_i^H), \tag{3.23}$$

is linear with respect to the variable Q_i. The second term,

$$(1-\alpha) \sum_{i=1}^{K} \log_2 \left| \mathbf{I} + \mathbf{h}_{ei} Q_i \mathbf{h}_{ei}^H \right|, \tag{3.24}$$

involves the logarithm of a determinant, where $\mathbf{I} + \mathbf{h}_{ei} Q_i \mathbf{h}_{ei}^H$ is an affine function of Q_i. Since the function $\log\det(X)$ is concave over the set of positive definite matrices [70], the second term is concave, not convex.

The constraint (3.22b) is convex due to its linearity, while (3.22c) ensures the positive semi-definiteness of Q_i, which defines a convex constraint set. Since the objective function is a weighted sum of a linear function and a concave function, it is generally not convex. However, if the problem is formulated as a *concave maximization problem with convex constraints*, it can be solved using convex optimization techniques. Hence, (3.22) is a convex optimization problem in the sense of maximizing a concave function over a convex feasible set.

3.3 Solution Approach

For some optimization problems, we can solve the problem using optimization techniques w.r.t. the corresponding i^{th} variable while all other variables are fixed and do so far

all variables iteratively until convergence. This method is known as a block coordinate ascent or descent algorithm [65].

Given the convexity of the problem in (3.22), we can easily verify that the optimization problem satisfies Slater's condition, ensuring a zero duality gap (i.e., strong duality) [70]. With the α values we can consider the two problems from (3.22).

Case 01: $0 \leq \alpha < 1$

The Lagrangian expression for the (3.22) is as follows:

$$\begin{aligned}\mathcal{L}(\{Q_i\}_{i=1}^K, \beta) = \quad & \alpha \sum_{i=1}^{K} \mathrm{tr}(\mathbf{M}\mathbf{c}_i Q_i \mathbf{c}_i^H) - \beta \left(\sum_{i=1}^{K} Q_i - P_{tx} \right) \\ & + (1-\alpha) \sum_{i=1}^{K} \log_2 \left| \mathbf{I} + \mathbf{h}_{ei} Q_i \mathbf{h}_{ei}^H \right|, \end{aligned} \tag{3.25}$$

where $\beta \geq 0$ is the Lagrangian variable. By using the properties of trace ($\mathrm{tr}(\mathbf{AB}) = \mathrm{tr}(\mathbf{BA})$) and the properties of determinant ($\det(\mathbf{I} + \mathbf{u}\mathbf{v}^H) = 1 + \mathbf{u}^H\mathbf{v}$) [71] we can simplify the (3.25) as follows:

$$\begin{aligned}\mathcal{L}(\{Q_i\}_{i=1}^K, \beta) = \quad & \alpha \sum_{i=1}^{K} \left(\mathbf{c}_i^H \mathbf{M} \mathbf{c}_i - \beta \right) Q_i + \beta P_{tx} \\ & + (1-\alpha) \sum_{i=1}^{K} \log_2 \left(1 + Q_i \mathbf{h}_{ei}^H \mathbf{h}_{ei} \right). \end{aligned} \tag{3.26}$$

From the stationary conditions for the (3.26), we can find a closed form solution for the Q_i upto one scalar, β as in

$$Q_i^* = \quad \left[\left(\frac{1-\alpha}{ln2} \right) \left(\frac{1}{\beta^* - \alpha \mathbf{c}_i^H \mathbf{M} \mathbf{c}_i} \right) - \frac{1}{\mathbf{h}_{ei}^H \mathbf{h}_{ei}} \right]^+. \tag{3.27}$$

Let the optimal solution be denoted by Q_i^*, $\forall i$ [1]. Then, the optimal closed-form solution upto one scalar for the downlink beamforming matrix can be written as,

$$\mathbf{R}_i^* = \quad \mathbf{c}_i Q_i^* \mathbf{c}_i^H. \tag{3.28}$$

[1]Note that $[x]^+ = max(0, x)$ to make sure that always satisfy the$x \geq 0$.

To determine the β^*, we can use any line search method. We provide the detailed steps for implementing this solution approach in **Algorithm 3,4**. The algorithm 3 is used to find the Lagrangian multiplier values for each weighted values. Here, we define 2 diagonal matrices to store corresponding downlink and dual uplink transmit covariance matrices and $\mathbf{b}^*$ is the output of this which includes all optimal Lagrangian variables input for the algorithm 4. The algorithm 4 is used to calculate optimal Q_i^* and $\mathbf{R}_i^*$ with corresponding weighted values. We defined new diagonal matrices to store optimal Q_i^* and $\mathbf{R}_i^*$ for each weighted values.

3.3.1 Analysis of Computational Complexity

In **Algorithm 3,4**, we examine the optimization algorithm for the multi-user scenario. In Part 1, initializing $\mathbf{c}_i$ has a complexity of $\mathcal{O}(N_t^3)$ due to the required matrix inversion. Computing $\mathbf{M}$ (as outlined in (3.19)) also has a complexity of $\mathcal{O}(N_t^3)$ because it involves matrix multiplication. The computational complexity of the third for loop (lines 10 to 17) is $K\mathcal{O}(N_t^3)$, as it involves matrix inversion and depends on the number of communication users K. Thus, the overall complexity of Part 1 is $(K+2)\mathcal{O}(N_t^3)$, which simplifies to $K\mathcal{O}(N_t^3)$. Similarly, Part 2 has a simplified complexity of $K\mathcal{O}(N_t^3)$. Therefore, the total computational complexity of **Algorithm 3,4** is $2K\mathcal{O}(N_t^3)$.

Algorithm 3 Calculation of β for given P_{tx}

Inputs: $\mathbf{M}$, $\mathbf{H}_K$, P_{tx}, β_{final}

Construct diagonal matrices $\mathbf{Q}$ and $\mathbf{R}$
for $\alpha = [0, 1)$ **do**
  for $\beta = 1, \ldots, \beta_{\text{final}}$ **do**
    Initialize $Q_i = 0, \ \forall i = 1, \ldots, K$
    Compute initial $\mathbf{c}_i^H$ as in **Appendix B**
    Compute initial $\mathbf{h}_{ei}^H \leftarrow \mathbf{h}_i^H \mathbf{A}_M^{-1/2}$ (See (3.11))
    for $i = 1$ to K **do**
      Compute Q_i using Eq. (3.27)
      Compute $\mathbf{R}_i$ using Eq. (3.28)
      Update $\mathbf{Q} \leftarrow Q_i$
      Update $\mathbf{R} \leftarrow \mathbf{R}_i$
      Update $\mathbf{h}_{ei}^H$ and $\mathbf{c}_i^H$
    end for
    $\mathbf{f} \leftarrow \text{tr}(\mathbf{Q})$
  end for
  Plot β vs $\mathbf{f}$
  Find β_α^* where $\text{tr}(\mathbf{Q}) = P_{tx}$ for α
end for
$\mathbf{b}^* \leftarrow \beta_\alpha^*$
return $\mathbf{b}^*$

Algorithm 4 Optimal Uplink Covariance Calculation

Inputs: $\mathbf{b}^*$, $\mathbf{M}$, P_{tx}, $\mathbf{H}_K$

Construct diagonal matrices $\mathbf{Q}_K$,$\mathbf{R}_K$, $\mathbf{Q}_{all}$ and $\mathbf{R}_{all}$
for $\alpha = (0, 1]$ **do**
  Initialize $Q_i = \mathbf{0}$, $\forall K$
  Compute initial $\mathbf{c}_i^H$ as in **Appendix B**
  Compute initial $\mathbf{h}_{ei}^H \leftarrow \mathbf{h}_i^H \mathbf{A}_M^{-1/2}$ (See (3.11))
  for $i = 1$ to K **do**
    Compute Q_i^* using Eq. (3.27) with $\mathbf{b}^*(\alpha)$
    Compute $\mathbf{R}_i^*$ using Eq. (3.28)
    Update $\mathbf{Q}_K \leftarrow Q_i$
    Update $\mathbf{R}_K \leftarrow \mathbf{R}_i$
    Update $\mathbf{h}_{ei}^H$ and $\mathbf{c}_i^H$
  end for
  $\mathbf{Q}_{all} \leftarrow \mathbf{Q}_K$
  $\mathbf{R}_{all} \leftarrow \mathbf{R}_K$
end for
return $\mathbf{Q}_{all}, \mathbf{R}_{all}$

3.4 Simulation Results

This section presents and analyzes the numerical results obtained for the case of multi-user communication.

3.4.1 Simulation Parameters

The parametric channel model [62], [63] is considered for the downlink users in the simulations. Under the system model, the channel response for the BS to k^{th} downlink user can be defined as:

$$\mathbf{h}_i = \sqrt{P_{Loss}} \sum_{q=1}^{Q_p} c_{i,q} \mathbf{a}_i(\theta_{i,q}); \quad i = 1, ..., K, \tag{3.29}$$

where Q_p is number of channel paths, $c_{i,q}$ denotes the channel path gain. Moreover, $\theta_{i,q}$ is an angle uniformly distributed over $[0, 2\pi]$ while P_{Loss} is the distance depends on path loss, and it is given by

$$P_{Loss} = \mathrm{P}_0 \left(\frac{d}{d_0} \right)^{\eta}, \tag{3.30}$$

where d_0 is the reference distance and η is the path loss exponent. Table 3.1 shows the basic simulation parameters used. For the simulations, we use MATLAB R2023a. For all simulations, we place the sensing object at a fixed location ($\theta_r = 0$).

Joint Beamforming for Multiple Users and Single Sensing Object

Fig. 3.2 illustrates the performance of optimal and sub-optimal beamforming designs as the number of communication users varies, with $N_t = N_r = 10$. In optimal beamforming, there are K beams, whereas sub-optimal beamforming employs $K + 1$ beams (as stated in **Proposition 3.1**). It is evident that as K increases, the gap between optimal and sub-optimal trade-offs decreases because increasing the number of communication users enhances system diversity and improves efficient resource allocation management, specifically transmit power. Consequently, the average system throughputs (MI and FI) for both beamforming designs converge to similar values, narrowing the performance gap between optimal and sub-optimal approaches.

Moreover, as more users position themselves closer to the sensing object, the likelihood of covering the target increases, further reducing the gap between optimal and

Table 3.1: Simulation parameters and values

Simulation Parameter	**Value**
Number of Communication users	K = 1,4,6,8
Transmit power	P_{tx} = 30 dBm
Noise variance	$\sigma_c^2 = \sigma_r^2 = 0$ dBm
Channel path numbers	$Q_p = 6$
Path-loss exponent	$\eta = 3.2$
Reference distance	$d_0 = 1$ m
Path-loss at the reference distance	P_0 = -30 dB
Operating frequency	3 GHz
Distance between two adjacent antennas	$\lambda/2$
Channel path gain	$c_{i,q} \sim \mathcal{CN}(0,1)$

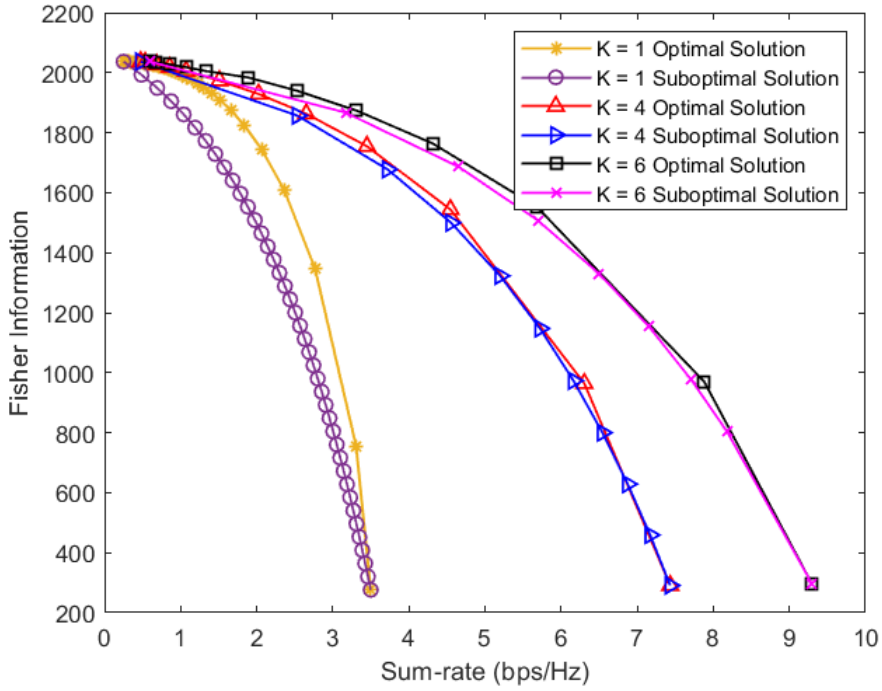


Figure 3.2: Comparison between optimal and sub-optimal beamforming for various numbers of users in terms of the trade-off between sum rate and Fisher Information

sub-optimal trade-offs. Therefore, with increasing numbers of communication users and constant N_t and N_r, the optimal and sub-optimal scenarios approach each other more closely.

Joint Beamforming for Multiple Users and Single Sensing Object With Transmitting and Receiving Antenna Variation

We illustrate the optimal and sub-optimal beamforming design with variations in N_r and N_t for $K = 4$. Fig. 3.3 demonstrates the optimal and sub-optimal variations for $N_r = N_t = 10$, $N_r = N_t = 16$, and $N_r = N_t = 20$. When we compare the gap between the optimal and sub-optimal results in these three scenarios, it is clear that the gap increases with increasing N_r and N_t. As the number of transmit and receive antennas increases, the beamforming design becomes more complex with higher

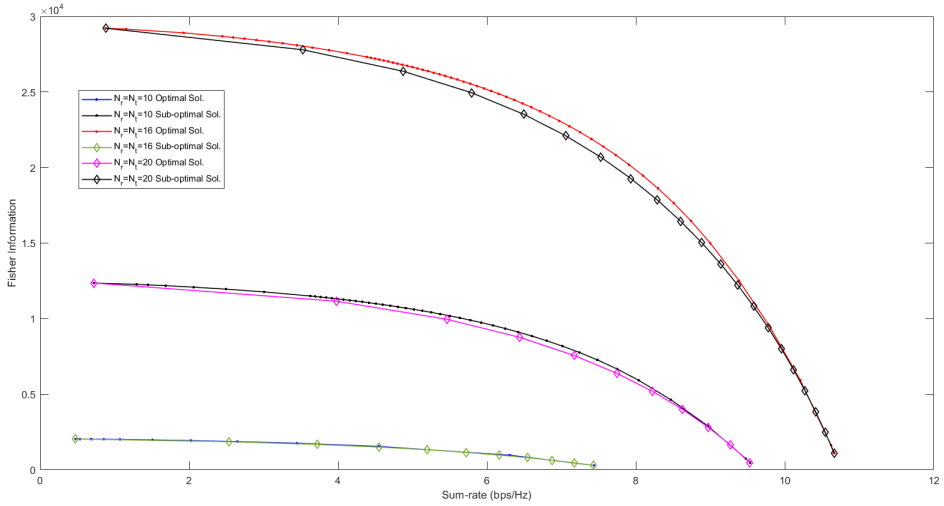


Figure 3.3: Comparison between optimal and sub-optimal beamforming for various numbers of transmitting and receiving antennas in terms of the trade-off between sum-rate and Fisher Information

degrees of freedom (DoF). Moreover, interference management and resource allocation have become more complex with many antennas. Then, for larger systems, optimal performances become increasingly superior to the sub-optimal performances. Therefore, as shown in Fig. 3.3, the gap between optimal and sub-optimal increases when N_r and N_t increase.

From the observations in 3.4.1 and 3.4.1, we can conclude that the case when the number of communication users increases with the constant number of transmitting and receiving antennas shows a weaker trade-off when compared to the trade-off with increasing number of transmitting and receiving antennas with the fixed number of communication users.

Variation in the Number of Communication Users

We analyze the Variation of the trade-off with the increasing number of communication users. According to Fig. 3.4 for $N_r = N_t = 10$, it is observed that the range of MI

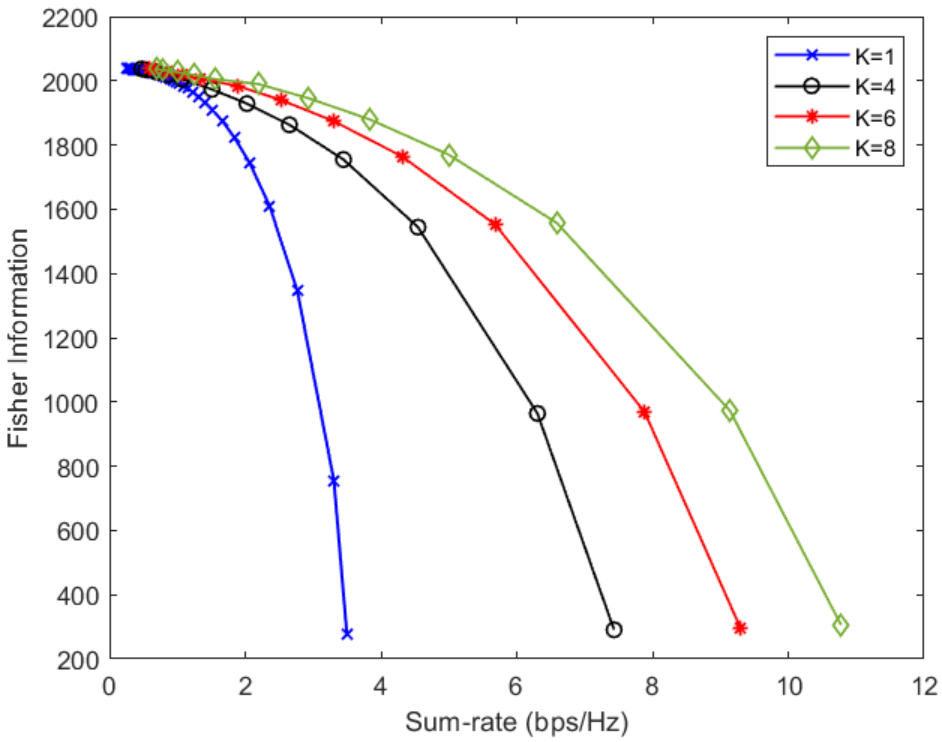


Figure 3.4: Variation of trade-off with number of communication users

increases as K increases. With fixed total power allocation, increasing the number of communication users leads to a higher MI (total sum rate) due to enhanced spatial diversity, increased DoF, and improved interference management.

Additionally, FI increases when the weighted value is 0. However, when the weighted value is 1, FI remains approximately constant due to increased communication users affecting the total FI, as shown in (3.12). When $\alpha = 1$, the optimization prioritizes FI, and given only one sensing object, there can be no increase or decrease in sensing performance. Therefore, FI remains constant when $\alpha = 1$.

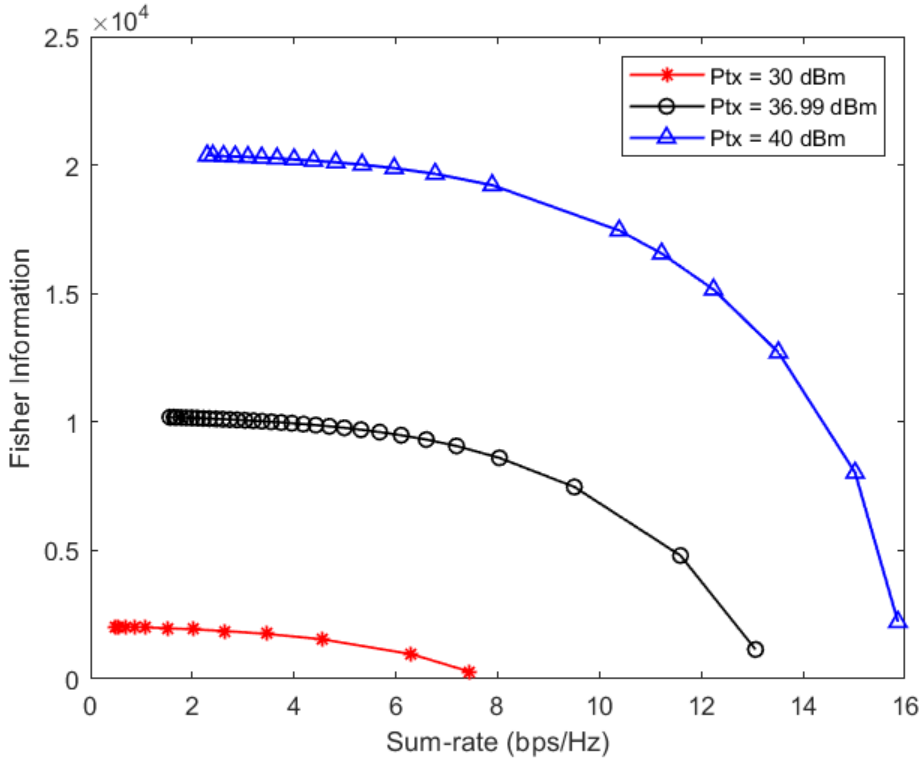


Figure 3.5: Variation of trade-off with transmit power budget

Transmit Power Budget Variation

We explore how variations in transmit power affect the trade-off between communication and sensing performance. Increasing transmit power in our model enhances performance by improving the signal-to-noise ratio (SNR), facilitating higher data rates and more precise target parameter estimation. It also extends the effective range for communication and sensing, enabling coverage for more distant users and detecting objects at greater distances. As depicted in Fig. 3.5, higher P_{tx} levels result in enhanced performance for both communication and sensing while also widening the range of variability for both FI and MI.

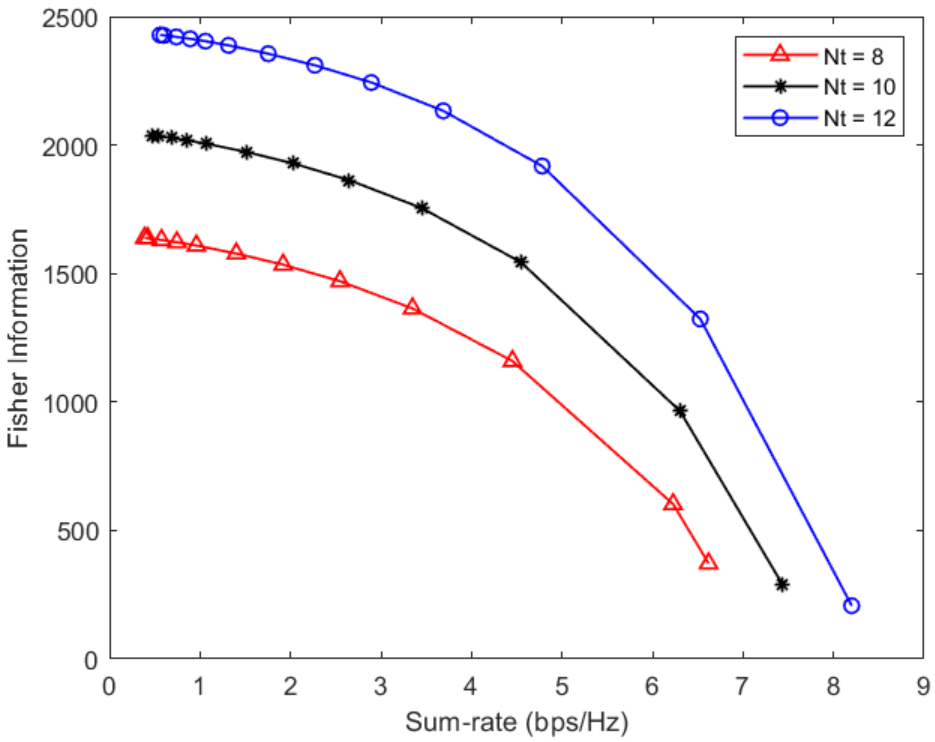


Figure 3.6: Variation of trade-off with number of transmitting antennas

Effect of Number of Transmitting Antennas

We investigate how the number of transmitting antennas influences the trade-off between MI and FI. Increasing the number of transmitting antennas in a communication system enhances MI and FI. Additional antennas increase spatial diversity, reducing interference and improving signal quality. This enhancement results in higher data rates and better SNR through techniques like spatial multiplexing and beamforming, which increases MI. Simultaneously, more antennas improve spatial resolution and parameter estimation accuracy, such as direction of arrival and channel state information. The extra antennas also enable advanced processing techniques that reduce noise and interference, thereby improving FI.

Fig. 3.6 shows the trade-off between MI and FI for $N_r = 10$ and $K = 4$. When

the weighted value is 0, we exclusively prioritize MI. At the same time, FI decreases because configurations that optimize MI may lead to higher interference and noise, which are detrimental to precise parameter estimation. When the weighted value is 1, MI approximately stabilizes, as the system's configurations that optimize FI do not necessarily support the highest possible data throughput while leading to enhanced sensing performance. This finding shows that increasing the number of transmitting antennas can simultaneously improve communication and sensing performances.

Variation in Number of Receiving Antennas

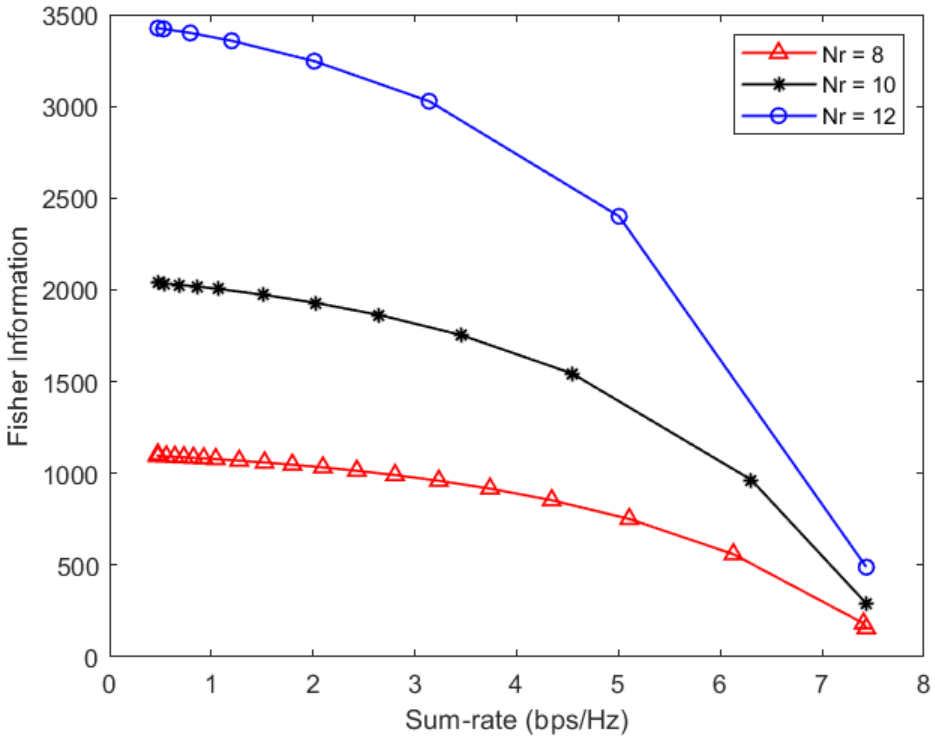


Figure 3.7: Variation of trade-off with number of receiving antennas

Fig. 3.7 demonstrates the trade-off with receiving antenna variation for $N_t = 10$ and $K = 4$. Increasing the number of receiving antennas (N_r) in a MIMO system affects

MI and FI differently. We can see that MI tends to reach a saturation range as N_t increases, especially under fixed transmit power conditions. This saturation occurs due to the efficient utilization of spatial diversity and multiplexing gains alongside practical limitations such as noise and interference. Conversely, FI continuously improves with more receiving antennas, enhancing parameter estimation precision by providing additional independent observations of the received signal. This finding underscores that enhancing sensing performance can be achieved by increasing the number of receiving antennas.

3.5 Chapter Summary

This chapter presented a comprehensive system model and analysis for a JCAS-enabled MIMO BS equipped with separate transmitting and receiving antenna arrays. The system model considered K single-antenna downlink users and a sensing object, with assumptions that LOS and NLOS conditions affect communication, while only LOS impacts sensing. The signal model for both downlink and uplink communication, as well as the sensing echo signal, was derived, incorporating beamforming vectors, channel responses, and noise models.

The chapter formulated a multi-objective optimization problem to maximize the weighted sum of MI for communication users and FI for the sensing object under a total power constraint. The problem was transformed using uplink-downlink duality, simplifying the optimization process. The convexity of the problem was established, and a block coordinate ascent algorithm was proposed to solve it efficiently. The computational complexity of the algorithm was analyzed, showing a dependency on the number of transmitting antennas and communication users.

Simulation results were presented to evaluate the performance of the proposed system under various scenarios, including variations in the number of communication users,

transmitting and receiving antennas, and transmit power budgets. Key findings include:

- **Optimal vs. Sub-optimal Beamforming:** As the number of communication users increases, the performance gap between optimal and sub-optimal beamforming narrows due to improved resource allocation and diversity.
- **Antenna Configuration Impact:** Increasing the number of transmitting and receiving antennas enhances both MI and FI, with FI showing continuous improvement while MI tends to saturate at higher antenna counts.
- **Transmit Power Variation:** Higher transmit power budgets improve both communication and sensing performance, expanding the range of achievable MI and FI.
- **User Diversity:** Increasing the number of communication users enhances MI due to spatial diversity and interference management, while FI remains stable when prioritizing sensing performance.

The chapter concludes that joint beamforming strategies are highly effective for JCAS systems, particularly in scenarios with multiple communication users and a single sensing object. The proposed optimization framework and algorithms provide a robust approach to balancing communication and sensing performance, demonstrating significant improvements in system efficiency and resource utilization.

Chapter 4

Conclusion and Future Directions

4.1 Conclusion

This thesis has explored the trade-off between communication and sensing in JCAS systems with multi-antenna configurations. We have proposed and analyzed optimal beamforming designs for single-user and multi-user scenarios while characterizing the Pareto boundary between MI and FI. Our findings demonstrate that a joint beamforming approach is optimal for JCAS, allowing for an efficient trade-off between communication and sensing performance.

In the first part of this thesis, we focused on a single-user, single-target scenario with a MIMO terrestrial base station. We formulated and solved a convex optimization problem to maximize the weighted sum of MI and FI under a total power constraint, deriving a closed-form optimal solution. Our results indicate that the optimal beamforming covariance matrix for JCAS is rank-one, confirming that joint beamforming is preferable over separate beamforming for communication and sensing. Furthermore, we extended our analysis to the case with EIRP constraints, illustrating how a decreasing EIRP leads to an optimal trade-off within a specific range of the weighting parameter

α. These results highlight the flexibility of our model in balancing communication and sensing objectives.

In the second part, we extended our study to a single-antenna multi-user scenario, considering the total transmit power constraint. We employed uplink-downlink duality conversion to simplify the optimization problem and used a block-coordinate ascent technique to obtain the optimal beamforming strategy. Our analysis revealed that strong joint beamforming occurs with more transmitting and receiving antennas rather than a more significant number of communication users with a fixed number of antennas. The results further validated that the optimal transmit covariance matrix has a rank equal to the number of communication users, reinforcing the superiority of joint beamforming for JCAS.

From a practical implementation perspective, our results provide key insights into designing JCAS systems that adaptively allocate resources to meet varying communication and sensing requirements. The derived optimal beamforming strategies offer computationally efficient solutions, making real-time adaptation feasible in dynamic wireless environments. Additionally, the demonstrated dependence of JCAS performance on the number of antennas rather than just the number of users suggests that practical deployment can benefit from intelligent antenna placement and array design. The impact of EIRP constraints further informs regulatory considerations for JCAS deployment in shared spectrum scenarios. These findings serve as a guideline for designing next-generation JCAS-enabled networks, ensuring a balance between communication efficiency and sensing accuracy.

Through extensive numerical simulations, we have characterized the Pareto boundary for different system settings, demonstrating the inherent trade-off between communication and sensing. Our findings provide a foundation for designing future JCAS systems that can dynamically adjust performance based on specific application needs.

4.2 Future Works

4.2.1 Advanced Optimization Methods

While convex optimization and block-coordinate ascent techniques provided efficient solutions for the scenarios studied, future work should explore more sophisticated optimization frameworks. For instance, machine learning-based approaches, such as deep reinforcement learning or meta-learning, could enable adaptive beamforming in highly dynamic environments with minimal prior assumptions. Additionally, distributed optimization methods could address scalability challenges in large-scale networks, while robust and stochastic optimization frameworks may better handle uncertainties in channel state information (CSI) or target mobility. Investigating low-complexity algorithms for real-time implementation would further enhance the practicality of JCAS systems.

4.2.2 Multi-User Multi-Target JCAS Scenarios

Extending the current single-target and multi-user models to a generalized multi-user multi-target framework is critical for real-world applications. This scenario introduces challenges such as inter-user interference, multi-target resolution, and resource allocation trade-offs between heterogeneous objectives. Novel beamforming designs must jointly optimize communication sum rates and multi-target sensing performance (e.g., tracking accuracy, and parameter estimation). Techniques like hierarchical optimization, interference alignment, or game-theoretic approaches could help balance competing demands. Furthermore, integrating radar-specific metrics, such as the probability of detection or false alarm rates, into the optimization framework would bridge gaps between communication-centric and radar-centric JCAS designs.

4.2.3 Near-Field JCAS Systems

Emerging technologies like ultra-massive MIMO, reconfigurable intelligent surfaces (RIS), and high-frequency (THz/Sub-THz) communications necessitate a shift from traditional far-field to near-field JCAS paradigms. Near-field beamforming requires spherical wavefront modeling, which fundamentally alters beam focusing, channel estimation, and sensing parameter extraction [72, 73]. Investigating how near-field effects influence the MI-FI trade-off, target localization precision, and communication reliability will be pivotal. Additionally, near-field JCAS could unlock applications such as ultra-precision sensing for human-computer interaction or industrial automation. Theoretical analysis and experimental validation of near-field joint beamforming strategies will be essential to harness these opportunities.

4.2.4 JCAS in Integrated Satellite-Terrestrial Networks (ISTN)

Future wireless networks will integrate terrestrial, aerial, and satellite communications, necessitating the development of JCAS techniques suited for space-based systems. One key challenge is designing beamforming strategies for satellite-based JCAS, where long propagation distances, atmospheric attenuation, and dynamic channel conditions significantly impact both communication and sensing performance [74, 75]. Additionally, UAVs and high-altitude platform systems (HAPS) are emerging as critical components of integrated networks, requiring adaptive JCAS beamforming techniques that can efficiently operate in highly dynamic environments [76, 77]. To fully harness the potential of ISTN-based JCAS, an advanced resource allocation framework must be developed to optimize power, spectrum, and beamforming across terrestrial, aerial, and satellite segments. This framework should account for challenges such as long propagation delays, non-stationary interference, and heterogeneous coverage requirements, ensuring efficient trade-offs between communication throughput and sensing accuracy in next-generation

wireless networks.

4.2.5 JCAS for Vehicular and Autonomous Systems

Vehicular JCAS can enhance situational awareness in autonomous systems by integrating sensing and communication in vehicle-to-everything (V2X) networks. Future work should focus on adaptive beamforming techniques that can handle high mobility and Doppler shifts, ensuring seamless connectivity and sensing in dynamic environments. Additionally, investigating mmWave and THz JCAS for automotive applications could unlock new capabilities, such as high-resolution vehicular radar and ultra-fast data transmission, improving autonomous navigation and safety. Multi-agent cooperative sensing, leveraging swarm intelligence, is another promising avenue that could enhance collaborative perception among connected vehicles and UAVs.

Appendix A

Derivation of the FIM

In this section, we describe the derivation method of the FI used in (2.6). With the assumption made in Section 2.1, we consider the statistically independent complex Gaussian of $\mathbf{y_r}$. The PDF of $\mathbf{y_r}$ with the unknown deterministic parameters $\mathbf{v} = [\theta_r \quad \gamma_r \quad \gamma_r^*]$ can be defined as:

$$p(\mathbf{y}_r; \mathbf{v}) = \frac{1}{(\pi\sigma_r^2)^{N_t}} \exp\left(-(\mathbf{y}_r - \gamma_r \mathbf{A}\mathbf{x}_{BC})^H (\sigma_r^2)^{-1} (\mathbf{y}_r - \gamma_r \mathbf{A}\mathbf{x}_{BC})\right). \tag{A.1}$$

As described in [58, 78, 79], we can find the log-likelihood function for the PDF in (A.1) as mentioned in (A.2) and the FI matrix $\mathbf{J}$ as in (A.6). Then, we can find the FI matrix concerning the i^{th} communication user as shown in (2.6).

$$\ln p(\mathbf{y}_r; \mathbf{v}) = -N_t \ln\left(\pi\sigma_r^2\right) - \frac{(\mathbf{y}_r - \gamma_r \mathbf{A}\mathbf{x}_{BC})^H (\mathbf{y}_r - \gamma_r \mathbf{A}\mathbf{x}_{BC})}{\sigma_r^2}. \tag{A.2}$$

We can find the derivatives with respect to parameters in $\mathbf{v}$ as follows:

$$\begin{aligned} \frac{\partial \ln(p)}{\partial \theta_r} = \frac{-1}{\sigma_r^2}\Big\{ & - \mathbf{y}_r \dot{\mathbf{A}}\mathbf{x}_{BC}\gamma_r + \gamma_r^H \gamma_r \mathbf{x}_{BC}^H \mathbf{A}\dot{\mathbf{A}}\mathbf{x}_{BC} \\ & -\gamma_r^H \mathbf{x}_{BC}^H \dot{\mathbf{A}}^H \mathbf{y}_r + \gamma_r^H \mathbf{x}_{BC}^H \dot{\mathbf{A}}^H \mathbf{A}\mathbf{x}_{BC}\gamma_r \Big\}, \end{aligned} \tag{A.3}$$

$$\frac{\partial \ln(p)}{\partial \gamma_r} = \frac{1}{\sigma_r^2}\Big\{(\mathbf{y}_r - \mathbf{A}\mathbf{x}_{BC}\gamma_r)^H \mathbf{A}\mathbf{x}_{BC}\Big\}, \tag{A.4}$$

$$\frac{\partial \ln(p)}{\partial \gamma_r^*} = \frac{1}{\sigma_r^2}\Big\{(\mathbf{A}\mathbf{x}_{BC})^H(\mathbf{y}_r - \mathbf{A}\mathbf{x}_{BC}\gamma_r)\Big\}. \tag{A.5}$$

From (A.3), (A.4), and (A.5), we can derive the Fisher information matrix using equation (A.6) below:

$$\mathbf{J} = \mathbb{E}\left(\left(\frac{\partial(\ln p(\mathbf{y}_r;\mathbf{v}))}{\partial \mathbf{v}}\right)\left(\frac{\partial(\ln p(\mathbf{y}_r;\mathbf{v}))}{\partial \mathbf{v}}\right)^T\right). \tag{A.6}$$

Appendix B

Proof of Proposition 3.1

Proof of Proposition 3.1

The dual uplink optimization problem in (3.22) is a convex optimization problem. Therefore, Slater's conditions verify a zero duality gap [70], [80]. Thus, we consider the Lagrangian function ($\mathcal{L}\left(\{Q_i\}_{i=1}^K, \mathbf{R}_0, \beta, \{\mu_i\}_{i=1}^K, \mathbf{Z}_0\right)$) for (3.22) as follows:

$$\begin{aligned}\mathcal{L} = \quad & \alpha \sum_{i=1}^{K} \left(\alpha \mathbf{c}_i^H \mathbf{M} \mathbf{c}_i - \beta + \mu_i\right) Q_i + \beta P_{tx} \\ & + \operatorname{tr}\left(\left(\alpha \mathbf{M} - \beta \mathbf{I}_{N_t} + \mathbf{Z}_0\right) \mathbf{R}_0\right) + (1-\alpha) \sum_{i=1}^{K} \log_2 \left|\mathbf{I} + \mathbf{h}_{ei} Q_i \mathbf{h}_{ei}^H\right|,\end{aligned} \tag{B.1}$$

where $\beta \geq 0, \mathbf{Z}_0 \succeq 0, \mu_i \geq 0; \forall i$.

Let's consider the **case 1:** $0 \leq \alpha < 1$. Optimal solutions of (B.1) should follow the complementary slackness conditions:

$$\mu_i Q_i^* = 0; \forall i = 1, .., K, \tag{B.2}$$

$$\operatorname{tr}\left(\mathbf{Z}_0 \mathbf{R}_0^*\right) = 0, \tag{B.3}$$

$$\beta \left(\sum_{i=1}^{K} Q_i^* + \mathrm{tr}(\mathbf{R}_0^*) - P_{tx} \right) = 0. \tag{B.4}$$

According to the (B.2), to satisfy the SINR requirements, it is confirmed that $Q_i^* \neq 0$ and $\mathrm{rank}(Q_i^*) = 1; \forall i$ and $\mu_i = 0$. From the (B.4) $\beta > 0$ to hold $\mathbf{Z}_0 \succeq 0$. Then, $\mathbf{R}_0^*$ must lie in the null space of $\mathbf{Z}_0$ to satisfy the (B.3). Therefore, $\mathbf{R}_0^* = \mathbf{0}$ and $\mathrm{rank}(\mathbf{Z}_0) \geq N_t - 1$. Because of these arguments, we can proof that when $0 \leq \alpha < 1$, the optimal solution satisfies the $\mathrm{rank}(Q_i^*) = 1; \forall i$ and $\mathbf{R}_0^* = \mathbf{0}$.

Let's consider the **case 1:** $\alpha = 1$.

At $\alpha = 1$, the constraint reduces to $\mathrm{tr}(\mathbf{Q}_i + \mathbf{R}_0) \leq P_{\max}$. Since the objective function (FI) is linear in $\mathbf{Q}_i$ and $\mathbf{R}_0$. The solution for this case is not unique. Any solution with rank 1, where the total power is pointing toward the sensing direction is optimum.

Preposition 3.1 is proven.

Appendix C

BC to MAC Transformation

Here, we explain the relationship between the downlink beamforming matrix and the uplink beamforming matrix. This transformation is performed on a user-by-user basis, ensuring equal uplink and downlink sum-rate capacity as indicated in (3.8) [65, 69]. Since the power budget is identical for both uplink and downlink, we have:

$$\sum_{i=1}^{K} Q_i = \sum_{i=1}^{K} \mathrm{tr}(\mathbf{R}_i). \tag{C.1}$$

The equivalent downlink covariance matrix $\mathbf{R}_i$ can be expressed as:

$$\mathbf{R}_i = \mathbf{T}_i^{-1/2} \mathbf{f}_i J_i S_i^{1/2} Q_i S_i^{1/2} J_i \mathbf{f}_i^H \mathbf{T}_i^{-1/2}, \tag{C.2}$$

where

$$\mathbf{T}_i = \mathbf{I} + \sum_{l=i+1}^{K} \left(\mathbf{h}_l Q_l \mathbf{h}_l^H \right), \tag{C.3}$$

$$S_i = 1 + \mathbf{h}_i^H \left(\sum_{l=1}^{i-1} \mathbf{R}_l \right) \mathbf{h}_i. \tag{C.4}$$

Furthermore, $\mathbf{T}_i^{-1/2} \mathbf{h}_i S_i^{1/2}$ is a vector, and its singular value decomposition (SVD) is straightforward, since $J_i = 1$. Then, with the simplified

$$\text{svd}\left(\mathbf{T}_i^{-1/2}\mathbf{h}_i S_i^{1/2}\right) = \mathbf{f}_i \mathrm{D}_i. \tag{C.5}$$

For the transformation, we start with $i = 1$. For simplicity, we define $\mathbf{c}_i \in \mathbb{C}^{1\times N_t}$ as follows:

$$\mathbf{c}_i = S_i^{1/2}\mathbf{f}_i^H \mathbf{T}_i^{-1/2}. \tag{C.6}$$

Bibliography

[1] F. Salahdine, T. Han, and N. Zhang, "5g, 6g, and beyond: Recent advances and future challenges," *Annales des Telecommunications/Annals of Telecommunications*, vol. 78, pp. 525–549, Oct. 2023.

[2] M. Liu, M. Yang, and A. Nallanathan, "On the performance of uplink and downlink integrated sensing and communication systems," in *2022 IEEE Globecom Workshops (GC Wkshps)*, pp. 1236–1241, 2022.

[3] F. Liu, Y. Cui, C. Masouros, J. Xu, T. X. Han, Y. C. Eldar, and S. Buzzi, "Integrated sensing and communications: Toward dual-functional wireless networks for 6g and beyond," *IEEE Journal on Selected Areas in Communications*, vol. 40, no. 6, pp. 1728–1767, 2022.

[4] F. Liu, C. Masouros, A. P. Petropulu, H. Griffiths, and L. Hanzo, "Joint radar and communication design: Applications, state-of-the-art, and the road ahead," *IEEE Transactions on Communications*, vol. 68, no. 6, pp. 3834–3862, 2020.

[5] A. R. Chiriyath, B. Paul, and D. W. Bliss, "Radar-communications convergence: Coexistence, cooperation, and co-design," *IEEE Transactions on Cognitive Communications and Networking*, vol. 3, no. 1, pp. 1–12, 2017.

[6] A. Al-Salehi, M. M. A.-E. Sufyan, A. N. Malik, and M. Al-Asaly, "A comprehensive survey of joint radar-communication technologies and their future applications in healthcare sector," *IEEE Access*, pp. 1–1, 2024.

[7] B. Li and A. P. Petropulu, "Joint transmit designs for coexistence of mimo wireless communications and sparse sensing radars in clutter," *IEEE Transactions on Aerospace and Electronic Systems*, vol. 53, no. 6, pp. 2846–2864, 2017.

[8] J. A. Mahal, A. Khawar, A. Abdelhadi, and T. C. Clancy, "Spectral coexistence of mimo radar and mimo cellular system," *IEEE Transactions on Aerospace and Electronic Systems*, vol. 53, no. 2, pp. 655–668, 2017.

[9] J. A. Zhang, F. Liu, C. Masouros, R. W. Heath, Z. Feng, L. Zheng, and A. Petropulu, "An overview of signal processing techniques for joint communication and radar sensing," *IEEE Journal of Selected Topics in Signal Processing*, vol. 15, p. 1295–1315, Nov. 2021.

[10] B. Paul, A. R. Chiriyath, and D. W. Bliss, "Survey of rf communications and sensing convergence research," *IEEE Access*, vol. 5, pp. 252–270, 2017.

[11] M. L. Rahman, P.-f. Cui, J. A. Zhang, X. Huang, Y. J. Guo, and Z. Lu, "Joint communication and radar sensing in 5g mobile network by compressive sensing," in *2019 19th International Symposium on Communications and Information Technologies (ISCIT)*, pp. 599–604, 2019.

[12] Y. Cui, F. Liu, X. Jing, and J. Mu, "Integrating sensing and communications for ubiquitous iot: Applications, trends, and challenges," *IEEE Network*, vol. 35, no. 5, pp. 158–167, 2021.

[13] N. Decarli, S. Bartoletti, and B. M. Masini, "Joint communication and sensing in 5g-v2x vehicular networks," in *2022 IEEE 21st Mediterranean Electrotechnical Conference (MELECON)*, pp. 295–300, 2022.

[14] N. C. Luong, X. Lu, D. T. Hoang, D. Niyato, and D. I. Kim, "Radio resource management in joint radar and communication: A comprehensive survey," *IEEE Communications Surveys & Tutorials*, vol. 23, no. 2, pp. 780–814, 2021.

[15] T. Wild, V. Braun, and H. Viswanathan, "Joint design of communication and sensing for beyond 5g and 6g systems," *IEEE Access*, vol. 9, pp. 30845–30857, 2021.

[16] L. Han and K. Wu, "Joint wireless communication and radar sensing systems – state of the art and future prospects," *IET Microwaves, Antennas &Amp; Propagation*, vol. 7, pp. 876–885, 2013.

[17] T. Perera, A. Mezghani, and E. Hossain, "On the characterization of pareto boundary for joint communication and sensing in mimo wireless systems," in *2024 IEEE International Conference on Communications Workshops (ICC Workshops)*, pp. 685–690, 2024.

[18] A. Zhang, M. L. Rahman, X. Huang, Y. J. Guo, S. Chen, and R. W. Heath, "Perceptive mobile networks: Cellular networks with radio vision via joint communication and radar sensing," *IEEE Vehicular Technology Magazine*, vol. 16, no. 2, pp. 20–30, 2021.

[19] J. A. Zhang, Y. J. Guo, and K. Wu, *Introduction to Joint Communications and Sensing (JCAS)*, pp. 1–30. John Wiley & Sons, Ltd, 2023.

[20] A. Hanif, S. Ahmed, T. Y. Al-Naffouri, and M.-S. Alouin, "Exploring the synergy: A review of dual-functional radar communication systems," 2023.

[21] P. Kumari, J. Choi, N. Gonzalez-Prelcic, and R. W. H. Jr, "Ieee 802.11ad-based radar: An approach to joint vehicular communication-radar system," 2017.

[22] R. C. Daniels, E. R. Yeh, and R. W. Heath, "Forward collision vehicular radar with ieee 802.11: Feasibility demonstration through measurements," *IEEE Transactions on Vehicular Technology*, vol. 67, no. 2, pp. 1404–1416, 2018.

[23] M. Bică and V. Koivunen, "Multicarrier radar-communications waveform design for rf convergence and coexistence," in *ICASSP 2019 - 2019 IEEE International Conference on Acoustics, Speech and Signal Processing (ICASSP)*, pp. 7780–7784, 2019.

[24] J. A. Zhang, M. L. Rahman, K. Wu, X. Huang, Y. J. Guo, S. Chen, and J. Yuan, "Enabling joint communication and radar sensing in mobile networks—a survey," *IEEE Communications Surveys & Tutorials*, vol. 24, no. 1, pp. 306–345, 2022.

[25] A. Hassanien, B. Himed, and M. G. Amin, "Transmit/receive beamforming design for joint radar and communication systems," in *2018 IEEE Radar Conference (RadarConf18)*, pp. 1481–1486, 2018.

[26] Y. Zhang, Q. Li, L. Huang, and J. Song, "Waveform design for joint radar-communication system with multi-user based on mimo radar," in *2017 IEEE Radar Conference (RadarConf)*, pp. 0415–0418, 2017.

[27] K. Wu, J. A. Zhang, X. Huang, Y. J. Guo, and R. W. Heath, "Waveform design and accurate channel estimation for frequency-hopping mimo radar-based communications," *IEEE Transactions on Communications*, vol. 69, no. 2, pp. 1244–1258, 2021.

[28] K. V. Mishra, M. Bhavani Shankar, V. Koivunen, B. Ottersten, and S. A. Vorobyov, "Toward millimeter-wave joint radar communications: A signal processing perspective," *IEEE Signal Processing Magazine*, vol. 36, no. 5, pp. 100–114, 2019.

[29] F. Liu, Y.-F. Liu, C. Masouros, A. Li, and Y. C. Eldar, "A joint radar-communication precoding design based on cramér-rao bound optimization," in *2022 IEEE Radar Conference (RadarConf22)*, pp. 1–6, 2022.

[30] T. Huang, X. Xu, Y. Liu, N. Shlezinger, and Y. C. Eldar, "A dual-function radar communication system using index modulation," in *2019 IEEE 20th International Workshop on Signal Processing Advances in Wireless Communications (SPAWC)*, pp. 1–5, 2019.

[31] A. Hassanien, M. G. Amin, E. Aboutanios, and B. Himed, "Dual-function radar communication systems: A solution to the spectrum congestion problem," *IEEE Signal Processing Magazine*, vol. 36, no. 5, pp. 115–126, 2019.

[32] Y. Chen, G. Liao, Y. Liu, H. Li, and X. Liu, "Joint subcarrier and power allocation for integrated ofdm waveform in radcom systems," *IEEE Communications Letters*, vol. 27, no. 1, pp. 253–257, 2023.

[33] X. Tian, T. Zhang, Q. Zhang, and Z. Song, "High accuracy doppler processing with low complexity in ofdm-based radcom systems," *IEEE Communications Letters*, vol. 21, no. 12, pp. 2618–2621, 2017.

[34] C. Sturm and W. Wiesbeck, "Waveform design and signal processing aspects for fusion of wireless communications and radar sensing," *Proceedings of the IEEE*, vol. 99, no. 7, pp. 1236–1259, 2011.

[35] C. B. Barneto, S. D. Liyanaarachchi, T. Riihonen, L. Anttila, and M. Valkama, "Multibeam design for joint communication and sensing in 5g new radio networks,"

in *ICC 2020 - 2020 IEEE International Conference on Communications (ICC)*, pp. 1–6, 2020.

[36] X. Chen, Z. Feng, Z. Wei, P. Zhang, and X. Yuan, "Code-division ofdm joint communication and sensing system for 6g machine-type communication," *IEEE Internet of Things Journal*, vol. 8, no. 15, pp. 12093–12105, 2021.

[37] S. M. Kay, *Fundamentals of statistical signal processing: estimation theory*. Prentice-Hall, Inc., 1993.

[38] A. Liu, Z. Huang, M. Li, Y. Wan, W. Li, T. X. Han, C. Liu, R. Du, D. T. K. Pin, J. Lu, Y. Shen, F. Colone, and K. Chetty, "A survey on fundamental limits of integrated sensing and communication," 2021.

[39] J. A. Zhang, F. Liu, C. Masouros, R. W. Heath, Z. Feng, L. Zheng, and A. Petropulu, "An overview of signal processing techniques for joint communication and radar sensing," *IEEE Journal of Selected Topics in Signal Processing*, vol. 15, no. 6, pp. 1295–1315, 2021.

[40] F. Liu, Y.-F. Liu, A. Li, C. Masouros, and Y. C. Eldar, "Cramér-rao bound optimization for joint radar-communication beamforming," *IEEE Transactions on Signal Processing*, vol. 70, pp. 240–253, 2021.

[41] J. Li, G. Zhou, T. Gong, and N. Liu, "A framework for mutual information-based mimo integrated sensing and communication beamforming design," *IEEE Transactions on Vehicular Technology*, vol. 73, no. 6, pp. 8352–8366, 2024.

[42] R. W. Heath Jr. and A. Lozano, *Foundations of MIMO Communication*. Cambridge University Press, 2018.

[43] C. E. Shannon, "A mathematical theory of communication," *The Bell System Technical Journal*, vol. 27, no. 3, pp. 379–423, 1948.

[44] Y. Peng, S. Yang, W. Lyu, Y. Li, H. He, Z. Zhang, and C. Assi, "Mutual information-based integrated sensing and communications: A wmmse framework," *IEEE Wireless Communications Letters*, vol. 13, no. 10, pp. 2642–2646, 2024.

[45] D. Cimini, F. Marzano, M. Biscarini, R. Gil, P. Schluessel, F. Concaro, M. Marchetti, M. Pasian, and F. Romano, "Applicability of the langley method for non-geostationary in-orbit satellite effective isotropic radiated power estimation," *IEEE Transactions on Antennas and Propagation*, vol. PP, pp. 1–1, 01 2021.

[46] F. Liu, Y.-F. Liu, A. Li, C. Masouros, and Y. C. Eldar, "Cramér-rao bound optimization for joint radar-communication beamforming," *IEEE Transactions on Signal Processing*, vol. 70, p. 240–253, 2022.

[47] H. Hua, T. X. Han, and J. Xu, "Mimo integrated sensing and communication: Crb-rate tradeoff," *IEEE Transactions on Wireless Communications*, vol. 23, no. 4, pp. 2839–2854, 2024.

[48] Y. Xiong, F. Liu, Y. Cui, W. Yuan, T. X. Han, and G. Caire, "On the fundamental tradeoff of integrated sensing and communications under gaussian channels," 2023.

[49] F. Liu, Y. Xiong, K. Wan, T. X. Han, and G. Caire, "Deterministic-random tradeoff of integrated sensing and communications in gaussian channels: A rate-distortion perspective," 2023.

[50] C. Ouyang, Y. Liu, and H. Yang, "Mimo-isac: Performance analysis and rate region characterization," *IEEE Wireless Communications Letters*, vol. 12, no. 4, pp. 669–673, 2023.

[51] C. Ouyang, Y. Liu, H. Yang, and N. Al-Dhahir, "Integrated sensing and communications: A mutual information-based framework," *IEEE Communications Magazine*, vol. 61, no. 5, pp. 26–32, 2023.

[52] C. Ouyang, Y. Liu, and H. Yang, "Performance of downlink and uplink integrated sensing and communications (isac) systems," *IEEE Wireless Communications Letters*, vol. 11, no. 9, pp. 1850–1854, 2022.

[53] L. Miretti, R. L. G. Cavalcante, E. Björnson, and S. Stańczak, "Ul-dl duality for cell-free massive mimo with per-ap power and information constraints," 2024.

[54] S. Zarei, W. Gerstacker, and R. Schober, "Uplink/downlink duality in massive mimo systems with hardware impairments," in *2016 IEEE International Conference on Communications (ICC)*, pp. 1–7, 2016.

[55] T. Endeshaw, B. K. Chalise, and L. Vandendorpe, "Mse uplink-downlink duality of mimo systems under imperfect csi," in *2009 3rd IEEE International Workshop on Computational Advances in Multi-Sensor Adaptive Processing (CAMSAP)*, pp. 384–387, 2009.

[56] K. M. Attiah and W. Yu, "Beamforming design for integrated sensing and communications using uplink-downlink duality," 2024.

[57] F. Liu, Y.-F. Liu, A. Li, C. Masouros, and Y. C. Eldar, "Cramér-Rao Bound Optimization for Joint Radar-Communication Beamforming," *IEEE Transactions on Signal Processing*, vol. 70, pp. 240–253, 2022.

[58] I. Bekkerman and J. Tabrikian, "Target Detection and Localization Using MIMO Radars and Sonars," *IEEE Transactions on Signal Processing*, vol. 54, no. 10, pp. 3873–3883, 2006.

[59] I. CVX Research, "CVX: Matlab software for disciplined convex programming, version 2.0." `https://cvxr.com/cvx`, Aug. 2012.

[60] J. Liu, Y. T. Hou, and H. D. Sherali, "Conjugate gradient projection approach for multi-antenna gaussian broadcast channels," 2007.

[61] R. Hunger, D. A. Schmidt, M. Joham, and W. Utschick, "A general covariance-based optimization framework using orthogonal projections," in *2008 IEEE 9th Workshop on Signal Processing Advances in Wireless Communications*, pp. 76–80, 2008.

[62] D. Wijekoon, A. Mezghani, and E. Hossain, "Phase shifter optimization in ris-aided mimo systems under multiple reflections," *IEEE Transactions on Wireless Communications*, pp. 1–1, 2024.

[63] M. L. Rahman, J. A. Zhang, X. Huang, Y. J. Guo, and R. W. Heath, "Framework for a perceptive mobile network using joint communication and radar sensing," *IEEE Transactions on Aerospace and Electronic Systems*, vol. 56, no. 3, pp. 1926–1941, 2020.

[64] J. A. Zhang, F. Liu, C. Masouros, R. W. Heath, Z. Feng, L. Zheng, and A. Petropulu, "An Overview of Signal Processing Techniques for Joint Communication and Radar Sensing," *IEEE Journal of Selected Topics in Signal Processing*, vol. 15, no. 6, pp. 1295–1315, 2021.

[65] N. Jindal, W. Rhee, S. Vishwanath, S. Jafar, and A. Goldsmith, "Sum power iterative water-filling for multi-antenna gaussian broadcast channels," *IEEE Transactions on Information Theory*, vol. 51, no. 4, pp. 1570–1580, 2005.

[66] W. Yu and J. Cioffi, "Sum capacity of gaussian vector broadcast channels," *IEEE Transactions on Information Theory*, vol. 50, no. 9, pp. 1875–1892, 2004.

[67] G. Caire and S. Shamai, "On the achievable throughput of a multiantenna gaussian broadcast channel," *IEEE Transactions on Information Theory*, vol. 49, no. 7, pp. 1691–1706, 2003.

[68] M. Costa, "Writing on dirty paper (corresp.)," *IEEE Transactions on Information Theory*, vol. 29, no. 3, pp. 439–441, 1983.

[69] S. Vishwanath, N. Jindal, and A. Goldsmith, "Duality, achievable rates, and sum-rate capacity of gaussian mimo broadcast channels," *IEEE Transactions on Information Theory*, vol. 49, no. 10, pp. 2658–2668, 2003.

[70] S. Boyd and L. Vandenberghe, *Convex Optimization*. Cambridge University Press, 2004.

[71] K. B. Petersen and M. S. Pedersen, "The matrix cookbook," 2008.

[72] H. Hua, J. Xu, and R. Zhang, "Near-field integrated sensing and communication with extremely large-scale antenna array," 2024.

[73] J. Cong, C. You, J. Li, L. Chen, B. Zheng, Y. Liu, W. Wu, Y. Gong, S. Jin, and R. Zhang, "Near-field integrated sensing and communication: Opportunities and challenges," *IEEE Wireless Communications*, vol. 31, no. 6, pp. 162–169, 2024.

[74] C. K. Sheemar, P. Thiruvasagam, W. U. Khan, S. Solanki, G. C. Alexandropoulos, J. Querol, J. Plachy, O. Holschke, and S. Chatzinotas, "Joint communications and sensing for 6g satellite networks: Use cases and challenges," 2025.

[75] M. Zhang, X. Yang, and Z. Bu, "Joint channel selection and spectrum sensing in integrated satellite-terrestrial networks," in *2023 IEEE 24th International Workshop on Signal Processing Advances in Wireless Communications (SPAWC)*, pp. 451–455, 2023.

[76] Y. Zuo, M. Yue, H. Yang, L. Wu, and X. Yuan, "Integrating communication, sensing and computing in satellite internet of things: Challenges and opportunities," 2023.

[77] M. B. Yilmaz, L. Xiang, and A. Klein, "Joint beamforming and trajectory optimization for uav-aided isac with dipole antenna array," in *2024 27th International Workshop on Smart Antennas (WSA)*, pp. 1–7, 2024.

[78] Z. Ben-Haim and Y. C. Eldar, "On the constrained cramÉr–rao bound with a singular fisher information matrix," *IEEE Signal Processing Letters*, vol. 16, no. 6, pp. 453–456, 2009.

[79] P. Stoica and T. Marzetta, "Parameter estimation problems with singular information matrices," *IEEE Transactions on Signal Processing*, vol. 49, no. 1, pp. 87–90, 2001.

[80] J. Xu, L. Liu, and R. Zhang, "Multiuser miso beamforming for simultaneous wireless information and power transfer," *IEEE Transactions on Signal Processing*, vol. 62, no. 18, pp. 4798–4810, 2014.